Universiteit Antwerpen

This item is the archived peer-reviewed author-version of:

Preparation of CuO/SBA-15 catalyst by the modified ammonia driven deposition precipitation method with a high thermal stability and an efficient automotive CO and hydrocarbons conversion

Reference:

Xin Qi, Papavasiliou Aggeliki, Boukos Nikos, Glisenti Antonella, Pui Ho Li Jerry, Yang Yong, Philippopoulos Constantine J., Poulakis Evangelos, Katsaros Fotis K., Meynen Vera, ...- Preparation of CuO/SBA-15 catalyst by the modified ammonia driven deposition precipitation method w ith a high thermal stability and an efficient automotive CO and hydrocarbons conversion

Applied catalysis : B : environmental - ISSN 0926-3373 - Amsterdam, Elsevier science bv, 223(2018), p. 103-115

Full text (Publisher's DOI): https://doi.org/10.1016/J.APCATB.2017.03.071

To cite this reference: https://hdl.handle.net/10067/1478530151162165141

uantwerpen.be

Institutional repository IRUA

ACCEPTED MANUSCRIPT

Preparation of CuO/SBA-15 catalyst by the modified ammonia driven deposition precipitation method with a high thermal stability and an efficient automotive CO and hydrocarbons conversion

Qi Xin[a,*], Aggeliki Papavasilou[b], Nikos Boukos[b], Antonella Glisenti[c], Jerry Pui Ho Li[d], Yong Yang[d] Constantine J. Philippopoulos[e], Evangelos Poulakis[e], Fotis K. Katsaros[b], Vera Meynen[a], Pegie Cool[a]

[a] Laboratory of Adsorption & Catalysis, University of Antwerp, Universiteitsplein 1, 2610 Wilrijk, Belgium.

[b] Institute of Nanoscience and Nanotechnology, National Center for Scientific Research Demokritos, Aghia Paraskevi, 153 10 Athens, Greece.

[c] Dipartimento di Scienze Chimiche, Università degli Studi di Padova, Via F. Marzolo, 1, 35131, Padova, Italy.

[d] School of Physical Science and Technology, ShanghaiTech University, Haike Road 100, Pudong, Shanghai 201210, China

[e] Chemical Process Engineering Laboratory, Department of Chemical Engineering, National Technical University of Athens, 9 Heroon Polytechniou Str., Zografos Camphs, Athens, 157 80, Greece.

[*] Corresponding author: qi.xin@uantwerpen.be; Tel.: +32-3-265-23-54

ACCEPTED MANUSCRIPT

Graphical abstract

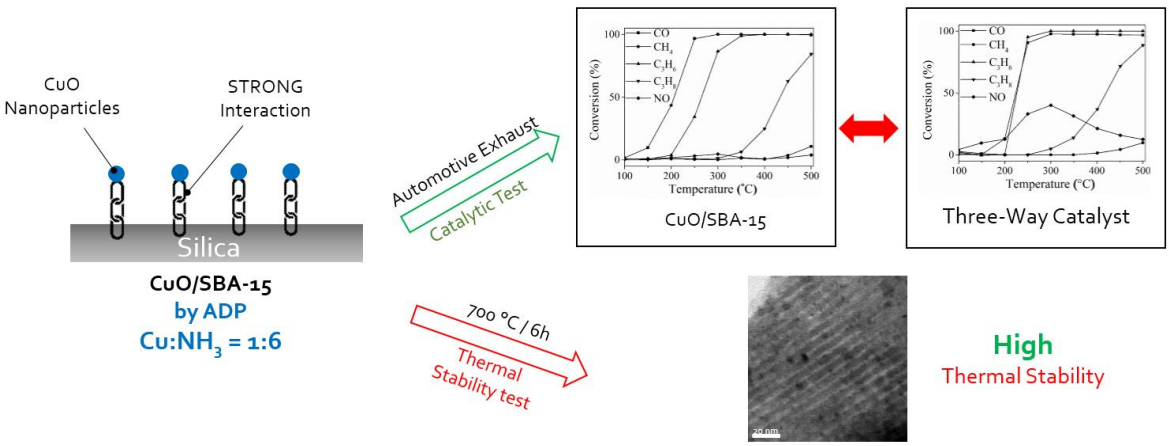

Highlights

- Ammonia based method for CuO/SBA-15 preparation with an outstanding Cu dispersion.
- Effect of Cu/NH_3 ratio on the copper dispersion and thermal stability.
- Cu based heterogeneous catalyst with an excellent automotive exhaust gas conversion.
- Cu based heterogeneous catalyst with a superior thermal stability.

Abstract

Copper oxide (CuO) loaded heterogeneous catalysts are a potential candidate to replace the critical precious metals Pt and Pd for the automotive oxidation reaction. However, a good CuO dispersion on the supports is necessary to compensate for its low intrinsic activity. Moreover, regarding the high operating temperature within the vehicle, a strong metal-support interaction is also required for providing a high thermal resistance to the catalyst. In this work, a series of CuO loaded SBA-15 catalysts has been prepared according to a modified ammonia driven deposition precipitation method (ADP). Herein, the Cu/NH_3 ratio of the synthesis has been varied with the aim to assess its influence on the CuO particles dispersion and CuO-support interaction. The morphology and porosity of the catalysts, the copper oxide dispersion and the chemical state of CuO were characterized and compared by a combination of techniques. In addition to this, the catalysts' thermal stability and their performance towards the automotive emission control have also been addressed. Results demonstrated that the ADP method is an efficient and scalable approach to fabricate a copper oxide based catalyst with a distinct automotive oxidation activity. Furthermore, it has been shown that, when a higher Cu/NH_3 ratio has been applied, a higher copper oxide dispersion degree can be achieved which has a strong metal-support interaction. The latter feature leads to its excellent thermal stability up to 700 °C, accompanied with a prolonged catalytic life-span in comparison with the conventional wet impregnation approach.

Keywords: Copper; ammonia driven deposition precipitation; high thermal stability; three-way catalyst

ACCEPTED MANUSCRIPT

1. Introduction

During the last decades, a significant increase in the development of copper oxide-based heterogeneous catalyst has been documented. The reason behind is its excellent redox property, low-cost and high recyclability, leading to its application in several industrial processes [1–3]. Furthermore, Kummer et al. even suggested its potential for replacing the precious metals for the automotive oxidation reactions [4]. The current three-way catalyst based on Pt, Pd and Rh effectively converts the hazardous CO, NO and hydrocarbons (HCs) originating from fuel combustion to less harmful CO_2, H_2O and N_2. Despite the high activity and durability, the rising scarcity and cost of the precious group metals (PGM) active elements drive research for a more common and economical beneficial alternative [5]. For this reason, CuO nanoparticles supported on a porous carrier form a promising candidate for automotive oxidation reactions. However, challenges arise for improving its activity and stability as CuO has an activity that is 50 times lower than that of Pd for CO oxidation and even 100 times lower than Pt for HCs conversion [4]. Secondly, due to its low melting point (1083 °C) and Tamann temperature (405 °C), the high reaction temperature within the catalyst (e.g. for automotive applications up to 800 °C) accelerates the particles migration and aggregation phenomena, resulting in catalyst deactivation and shortening its life-span [6–9]. In order to overcome these obstacles, literature emphasizes the importance of a well-designed metal deposition method affording highly dispersed active sites and a strong metal-support interaction [10,11]. On the other hand, its industrial applicability and environmental impact also need to be taken into account, regarding the high production volumes and rates of the vehicle exhaust catalyst for the automobile industry [12].

Recently, preparations involving the adsorption of copper tetra-amine complex ($Cu(NH_3)_4(H_2O)_2^{2+}$) has been widely applied as a simple and efficient copper oxide deposition strategy [13]. Methods such as selective adsorption (SA), ammonia evaporation (AE) and ammonia driven deposition precipitation (ADP) are all categorized under this approach [14–17]. During the synthesis, a certain amount of ammonia is added into an aqueous solution containing a Cu^{2+} precursor and the support material, followed by a thermal activation treatment (calcination and/or reduction). Catalysts prepared through this procedure demonstrate a high dispersion state of copper oxide particles onto the support. Moreover, Toupance et al. postulates the existence of two types of copper oxide species within the material, namely grafted Cu^{2+} and copper phyllosilicate [18]. The latter material is a type of copper silicate with a lamellar structure, wherein the layers of SiO_4 tetrahedra were sandwiched between discontinuous layers of CuO_6 octahedra [17–19]. A large number of studies reported the superior thermal behavior of copper phyllosilicate due to a strong metal-support interaction. For example, Zhu et al. successfully synthesized a Cu/SiO_2 catalyst with a dominant copper phyllosilicate phase by using a modified ammonia evaporation hydrothermal (AEH) method. This method leads to the formation of a pure-phase copper phyllosilicate which is stable upon heat treatment at 400 °C [20]. Also, Yue et al. prepared a copper phyllosilicate nanotube sheath by using hydrolytic adsorption method with a significant reactivity and stability [21].

Although considerable research has been focused on maximizing the copper phyllosilicate phase in the catalysts, less attention has been paid to the structural and catalytic property of the grafted copper oxide species. In the current study, we investigated the automotive catalytic performance, durability and thermal stability of a CuO/SBA-15 catalyst with a dominant grafted Cu^{2+} phase. This catalyst has been realized by modifying the ADP method developed by Guo et al. [22,23]. During the synthesis, we varied the Cu^{2+}/NH_3 ratio while keeping the solution's pH at a fixed value. In this way, CuO-loaded

ACCEPTED MANUSCRIPT

catalysts with a different CuO dispersion and metal-support interaction have been realized. This leads to their divergent behavior towards the automotive emission control, in particular the catalysts' thermal stability. The emphasis of this work is to assess the influence of the Cu^{2+}/NH_3 ratio on the different CuO phases formed, as well as its effect on the catalytic activity and life-span.

2. Experimental

2.1 Synthesis of the support SBA-15 silica

Mesoporous silica (SBA-15) was synthesized according to its verified synthesis [24]. Pluronic P123 triblock copolymer (P123, molecular weight 5800 g/mol, Sigma Aldrich) was first dissolved in an 1 M aqueous solution of HCl (37 wt.%, Acros) at 30 °C. After the copolymers' dissolution, the temperature was raised to 40 °C. Subsequently, tetraethyl orthosilicate (TEOS, Sigma Aldrich) was added drop wise into the solution under vigorous stirring. The molar composition of the synthesis gel is 1.0 TEOS/0.017 P123/2.1 HCl/116 H_2O. After 24 h of stirring, the mixture was hydrothermally treated at 100 °C for 72 h. The obtained solid was filtered and washed with deionized water and dried at 60 °C overnight. Finally, the material was calcined at 550 °C for 6 h with a heating rate of 1 °C/min in ambient air.

2.2 Catalysts preparation

2.2.1 Ammonia driven deposition precipitation method

For the synthesis of CuO/SBA-15 catalysts, we modified the method described by Guo et al. and altered the Cu^{2+}/NH_3 ratio at constant pH [15,23]. Firstly, ammonia (NH_4OH, 28-30 %, Sigma Aldrich) was added into the vial containing 0.19 g of copper nitrate ($Cu(NO_3)_2.3.H_2O$, >99 %, Merck) in order to obtain a molar Cu^{2+}/NH_3 ratio of respectively 1/3, 1/4 and 1/6. After that, respectively 5 mL, 10 mL and 25 mL de-ionized water was added into the solutions in order to obtain a fixed pH value of 10.6 for all syntheses but with a different absolute amount of ammonia. Subsequently, 0.5 g of SBA-15 support was suspended into the solution to achieve a 10 wt.% final Cu loading. The suspensions were then stirred for 48 h at room temperature, followed by a drying step at 60 °C overnight. Finally, the dried samples were calcined at 550 °C for 6 h with a heating rate of 1 °C/min. The synthesized catalysts were denoted as CS-13, CS-14 and CS-16.

2.2.2. Wet impregnation method

As a benchmark for the catalytic activity, a CuO/SBA-15 catalyst with the same amount of CuO loading has also been prepared by the conventional wet impregnation method. 0.5 g of SBA-15 support was suspended into a 25 mL solution containing 0.19 g copper nitrate ($Cu(NO_3)_2.3.H_2O$, >99 %, Merck). After 48 h stirring at room temperature, the suspension was dried at 60 °C overnight, followed by a calcination step at 550 °C for 6 h with a heating rate of 1°C/min. The prepared catalyst was denoted as CS-WI.

2.3 Characterization

N_2-physisorption was carried out with a Quantachrome Quadrasorb SI automated gas adsorption system. Prior to the measurements, the samples were outgassed at 200 °C for 16 h. The specific area was calculated using the Brunauer-Emmet-Teller (BET) equation. For the metal loaded samples, the specific area was calculated by excluding the metal content in the total sample weight. The Barret-Joyner-Halenda method was applied to estimate the pore size distribution. The total pore volume was determined at P/P_0= 0.95 while the micropore volume was obtained via the t-plot method.

ACCEPTED MANUSCRIPT

Wide angle X-ray diffraction was performed using a Rigaku rotating anode X-ray generator (operating at 50 kV, 100 mA, Ni-filtered CuK_{a1} radiation) and an R-AXIS IV image plate. Samples were sealed in Lindemann capillaries.

CuO dispersion of the catalysts was estimated by using the N_2O pulse titration method based on the following reaction: $2Cu + N_2O\ (g) \rightarrow Cu_2O + N_2\ (g)$ [25]. The measurement was performed in a tube furnace equipped with a Pfeiffer PrismaPlus mass spectrometer. Before the measurement, the sample was first reduced in a flow of 10 % H_2/Ar (flow rate 20 mL/min) at 500 °C for 10 minutes. After reduction, the sample was cooled down to 100 °C and flowed with pure Ar flow for 10 minutes in order to remove the H_2 from the surface. Subsequently, the titration was performed at 100 °C using a 0.5 % N_2O/Ar flow of 20 mL/min. The amount of active sites on the CuO surface was calculated by using the amount of N_2 produced during titration. Herein, a stoichiometric Cu:N_2 ratio of 2:1 should be taken into account. The CuO dispersion has then been determined by using the following equation (Eq. 1):

$$\text{Dispersion}\ (\%) = \left(\frac{2 \times N_2 \text{ molecules desorbed (mol)}}{\text{Total amount of Cu in sample (mol)}}\right) \times 100 \qquad \text{(Equation. 1)}$$

The average CuO particle size was estimated by assuming a spherical shape of the CuO particles. The reduction temperature of 500 °C has been chosen based on N_2O titration experiments over CS-16 catalysts reduced at different temperatures. The maximum active CuO surface increases from 200°C to 500°C, while it decreases again from 500 - 700°C, indicating either sintering and/or CuO aggregation (Supplementary Information 1).

The total amount of Cu was determined by electron probe microanalysis (EPMA) on a JEOL JXA 733. The powder materials were grinded and dispersed on a copper grid coated with a carbon film. For each sample, three measurement points were averaged to calculate the metal loading.

Diffuse Reflectance Infrared Fourier Transform (DRIFT) spectra were recorded on a Nicolet 6700 Fourier Transform IR spectrometer, equipped with an electromagnetic source in the mid-IR region (4000-400 cm^{-1}). The detector was a deuterated triglycine sulfate (DTGS) detector. The resolution was 4 cm^{-1} and for each spectrum, 200 scans were collected. The sample holder contained a 2 wt.% diluted sample in KBr and was measured under vacuum at room temperature.

Temperature programmed reduction (TPR) measurements of the catalysts were performed on a Quantachrome iQ. Prior to the measurement, about 20 mg of the sample was outgassed at 200 °C for 16 h. After cooling, the sample was first pretreated at 250 °C under a He flow for 1 h. Subsequently, the sample was reduced with 5 % H_2/Ar at a flow rate of 25 mL/min and the temperature was raised from 100 °C to 800 °C with a heating rate of 10 °C/min. The hydrogen consumption was continuously monitored using a thermal conductivity detector (TCD). The final TCD signal was normalized by the catalyst weight used during the measurement.

UV-Vis diffuse reflectance (UV-Vis-DR) analysis was carried out on a Nicolet Evolution 500 spectrophotometer equipped with an integrating sphere. The spectra were taken in the range of 200-800 nm with a scan speed of 120 nm/min. The samples were diluted to 2 wt.% with dried KBr.

X-ray photoelectron spectroscopy (XPS) was carried out by means of a PerkinElmer PHI 5600ci Multi Technique System, using AlK_α radiation (1486.6 eV) working at 250 W. The spectrometer was calibrated by assuming the binding energy (BE) of the Au $4f_{7/2}$ line to be 84.0 eV with respect to the Fermi level. Both extended spectra (survey – 187.85 eV pass energy, 0.5 eV/step, 0.05 s/step) and detailed spectra (for Cu2p, Si2p, O1s and C1s – 11.75 eV pass energy, 0.1 eV/step, 0.1 s/step) were collected. The standard deviation in the BE values of the XPS line is 0.10 eV. The atomic percentage, after a Shirley-type background subtraction was evaluated by using the PHI sensitivity factors. The peak positions

ACCEPTED MANUSCRIPT

were corrected for the charging effects by considering the C1s peak at 285.0 eV and by evaluating the BE differences.

TEM analysis was performed by utilizing a FEI CM20 TEM operating at an accelerating voltage of 200kV. Samples for TEM were prepared by suspending the sample in ethanol and drop casting it on a carbon coated Cu grid. Samples' morphological investigation was conducted with a JEOL JSM 7401F Field Emission Scanning Electron Microscope equipped with Gentle Beam mode. The applied acceleration voltage was 2 kV. Samples were mounted on metallic (brass) substrates using a double coated carbon conductive tape.

2.4 Thermal stability test

The thermal stability of the synthesized materials was tested using a Lenton furnace. Samples were exposed to a temperature of 700 °C for 6 h with a heating rate of 10 °C/min under ambient air.

2.5 Catalytic tests

The catalytic performance of the materials was tested in a fixed bed continuous flow stainless steel reactor with a gas hourly space velocity of 60 000 h^{-1} and a total gas flow rate of 200 NmL/min. Prior to the measurement, the catalytic powder was pelletized using an IR pelletizer and crushed in order to have a particle size between 500 µm and 1000 µm. The pressure applied to the pelletizer was about 200 MPa which does not affect the textural property of the material [26]. Afterwards, 200 mg of the sieved catalytic powder was pretreated by passing atmospheric air (50 mL/min) through the reactor at 500 °C (5 °C/min) for 2 h. Subsequently, the reactor was cooled to 50 °C and the catalyst was then exposed to vehicle exhaust gas under stoichiometric condition followed by heating to 500 °C with a heating rate of 5 °C/min and the conversion performance was recorded every 50 °C. The catalytic activity/stability in function of time-on-stream of the materials was assessed by monitoring the pollutants conversion at a constant temperature of 700 °C for 8 hours. The gas composition is listed in Table 1. For the analysis of the gas stream leaving the reactor, a Shimadzu GC-17A gas chromatograph equipped with an FID detector was used for the hydrocarbons conversion analysis. While a Dräger X-am 7000 CO analyzer was utilized for the CO gas quantification. A Thermo Scientific NOx analyzer was applied to monitor the NO conversion during the catalytic reaction. The catalytic activity of the catalysts was calculated from the conversion of respectively CO, CH_4, C_3H_6, C_3H_8 and NO in function of the reaction temperature. Light-off temperature (T_{50}) of the different components was obtained by taking the reaction temperature where a 50 % conversion was reached. For the comparison, a commercial precious metals loaded three-way catalyst (TWC), provided by Johnson Matthey, has also been tested. In order to obtain a comparable result with the powder catalyst, this TWC has been crushed to have a particle size between 500 µm and 1000 µm.

3. Results

3.1 Physicochemical properties

Textural properties of the synthesized catalysts were determined using N_2-sorption analysis, the respective isotherms are illustrated in Figure 1. Additionally, the structural properties derived from the materials' isotherms are summarized in Table 2. For comparison, the data of the pure SBA-15 support is also shown in the figure. The silica support demonstrates a type IV isotherm according to the IUPAC classification, accompanied by a H1 type hysteresis [27]. After CuO deposition, the shape of the hysteresis loop is preserved, showing the negligible impact of the method towards the materials' pore uniformity. However, a significant pore enlargement took place after metal loading and calcination,

ACCEPTED MANUSCRIPT

which is expressed by the increase in the average pore diameter for all samples. This phenomenon is originating from the dissolution of the silica's outer layer to silicic acid brought by the basic solution. Surprisingly, despite the same pH value of all samples, a positive trend in the pore size enlargement can be observed when the Cu/NH_3 ratio rises. This is correlated to the absolute amount of free OH^- ions within the solution during the metal deposition, which will be discussed in section 4.2. Apart from this, the CuO loaded samples display a drastic decrease in the surface area of about 40 %, accompanied by a significant loss of the total pore volume (micro- and mesoporosity). This is described by Prieto et al. as the confinement of the fine metal particles inside the support's pores [28].

3.2 Copper oxide characterization

DRIFT measurements have been performed to exclude the presence of phyllosilicate, since this phase gives a typical signal at respectively 670 cm^{-1} and 1027 cm^{-1} [18]. However, during the measurement, the presence of traces of atmospheric CO_2 (band at 671 cm^{-1}) will partly overlap with the phyllosilicate's δ_{OH} signal (at 670 cm^{-1}) and thus significantly affects the final result. For this reason, we applied a vacuum DRIFT measurement in order to minimize this effect. Figure 2 shows the vacuum-DRIFT spectra of the uncalcined Cu^{2+}/SBA-15 because the high calcination temperature will lead to the decomposition of the formed phyllosilicate [18]. All samples show characteristic bands at 806 cm^{-1}, 1080 cm^{-1} and 1290 cm^{-1} which can be assigned to the various vibration modes of Si-O bond in the amorphous SiO_2. When comparing with the spectrum of the pure SBA-15, the three catalysts exhibit a δ_{OH} band at 680 cm^{-1}, which is ascribed to the structural OH groups of copper nitrate hydroxide and the bands situated between 1300 cm^{-1} and 1420 cm^{-1} are ascribed to the molecular vibration of nitrate on the samples. Apart from this, $Cu(OH)_2$ is also present on the uncalcined catalysts which is characterized by its δ_{OH} band at 938 cm^{-1}. Based on the result, it can be noticed that neither characteristic δ_{OH} nor ν_{SiO} bands of phyllosilicate can be distinguished for any of the samples, which strongly indicates its absence on the catalysts. However, the existence of phyllosilicate in the catalysts cannot be completely excluded due to the possible overlapping of its δ_{OH} band with the δ_{OH} band of copper nitrate hydroxide at 680 cm^{-1}.

The copper species dispersion degree and the particle size of CuO clusters were estimated by both N_2O pulse titration and XRD analysis (Table 2). These two techniques are complementary to each other since XRD can only detect CuO crystals with sizes above a certain limit while N_2O pulse titration provides the dispersion degree and average particle size of all accessible Cu species on the catalyst. The N_2O pulse titration result shows a positive effect of the NH_3 amount on the Cu dispersion on the surface. In particular, it can be observed that the CS-14 and CS-16 samples have a comparable Cu dispersion (about 8 %) while it is much lower for CS-13 (2.5 %). Based on these data, the average Cu particle size has been calculated, which is respectively 11.9 nm and 12.4 nm for CS-14 and CS-16 while it is 40.7 nm for CS-13. On the other hand, the sample prepared by the WI method shows a poor dispersion degree (0.15 %) and a large Cu particle size (660 nm). However, caution must be taken when interpreting the N_2O results, given that the pre-reduction treatment, performed at high temperature (500 °C), could engender aggregation phenomena. Hence, results should be interpreted as a relative trend among the samples rather than an absolute value. The impact of pre-treatment temperature (200°C-700°C) on the CS-16 sample is demonstrated in the supplementary section. Additional information about the size and the presence of CuO crystals were provided by wide angle XRD analysis (Figure 3). The three sharp peaks at 2θ = 35.5°, 38.7° and 48.5°, which are superimposed on the broad signal of the silica support, are characteristic for CuO (tenorite) crystals on the materials. When looking into more detail, one can clearly observe the weaker CuO diffraction peaks for the CS-16 sample. Particle size calculation based on the Scherrer formula (Table 2) has been performed for the CuO (111) reflection, which gave 28 nm, 22 nm and 23 nm for CS-WI, CS-13 and CS-14 respectively, while it could

ACCEPTED MANUSCRIPT

not be estimated for CS-16. Another important aspect to mention here is the fact that the broad diffraction peaks characteristic for copper phyllosilicate (at 2θ = 30.5 and 35.8) are not present in any of the catalysts [14,18,29], which is in line with the result observed from the DRIFT spectra. The absence of copper phyllosilicate might be the result of its decomposition during the samples' calcination at 550 °C [18].

It can be seen that despite the larger copper oxide crystallites observed in XRD, the CS-14 sample possesses a similar copper dispersion degree and average particle size as the CS-16 sample. Hence, it can be derived that the CS-14 sample contains also very small CuO clusters besides some large CuO crystals (evidenced by XRD), that together resulted in a smaller average particle size, detectable only by N_2O chemisorption technique. On the other hand, CS-16 mainly consists of more uniform highly dispersed XRD silent CuO particles, with only a small amount of bulk CuO resulting in a similar dispersion degree and estimated particle size (N_2O titration) as in the CS-14.

X-ray photoelectron spectroscopy (XPS) was applied to elucidate the Cu oxidation state and the composition on the catalysts' surface. Figure 4 illustrates the Cu $2p_{3/2}$ core level signal of the samples which shows a high similarity between all spectra. In particular, all samples contain a main Cu $2p_{3/2}$ signal which is a contribution of mainly two peaks, located respectively at 933.5-934.0 eV and 935.9-936.1 eV. Both signals are attributed to the Cu^{2+} species on the material, evidenced by the characteristic shakeup satellite at 942 – 945 eV. The former peak at 933.5-934.0 eV is ascribed to Cu^{2+} species on the material in the form of CuO, while the peak at 935.9-936.1 eV is indicative for CuO species that are interacting with the support matrix [30]. Studies involving the ammonia based impregnation method often ascribe this latter peak to the copper phyllosilicate on the materials [14,20,31]. However, since both XRD and DRIFT results suggested the absence of phyllosilicate, the presence of grafted CuO would be more plausible in our case. The relative peak intensity of the Cu$2p_{3/2}$ signals is summarized in Table 3. An increasing contribution of the 935.9-936.1 eV peak can be observed when the molar Cu^{2+}/NH_3 ratio during the synthesis rises, which indicates a higher fraction of CuO species with a strong metal-support interaction. On the other hand, the characteristic shakeup satellite can also be deconvoluted into two individual peaks, located respectively at 941.6-942.6 eV and at 944.4-944.9 eV. The satellite peak at a lower BE is associated with Cu^{2+} in bulk CuO particles while the peak at 944.4-944.9 eV is attributed to well dispersed Cu^{2+} [32,33]. Hence, Cu^{2+} species in the form of both the bulk CuO and well dispersed CuO were observed on the materials' surface, which is in accordance with the XRD and N_2O results, although fewer differences can be deduced from XPS. The O1s and Si2p spectra of the samples show typical BE attributed respectively to –OH (533 eV) and SiO_2 on the surface of SBA-15 (Supplementary 2). Since no further significant differences can be observed in the latter two spectra, they will not be further discussed.

By combining the XRD, N_2O and XPS results, it can be concluded that the ADP method provides well dispersed CuO on the SBA-15 support with the existence of several types of CuO. Furthermore, the presence of a CuO phase with a strong metal-support interaction has been pointed out. We ascribe these CuO species to grafted CuO since no evidence of copper phyllosilicate can be observed. To further elucidate the structural differences of the CuO phases, UV–Vis diffuse reflectance (UV–Vis-DR) and temperature programmed reduction (H_2-TPR) measurements were carried out.

Figure 5 displays the UV-Vis-DR spectra of the calcined CuO/SBA-15 samples. Generally, four different absorption bands can be distinguished among the catalysts. The band centered at around 230 nm and 253 nm are both ascribed to the charge-transfer between mononuclear Cu^{2+} and oxygen. Studies suggest that the difference of the absorption wavelength between both CuO species is originating from their deviations in coordination and metal-substrate interaction [34,35]. The band centered at about 300 nm is attributed to the presence of $[Cu–O–Cu]_n$-type clusters (oligomeric species) different from

ACCEPTED MANUSCRIPT

the bulk CuO [36]. Finally, the signal at around 670 nm corresponds to the d–d transition of Cu^{2+} situated in an octahedral environment, which is the typical band for bulk CuO [37]. Generally, it can be seen that the CS-WI sample exhibits a higher amount of large CuO particles, evidenced by a stronger signal for oligomeric and bulk CuO species. Conversely, the latter signal is weak in the case for the samples prepared by the ADP method. By comparing the ADP samples, one can clearly observe some similarities. In particular, all samples exhibit a good CuO dispersion where the majority of CuO is present in mononuclear and oligomeric CuO species. However, the d-d transition band at 670 nm for CS-13 and CS-14 sample indicates the presence of bulk CuO, which is in line with the XRD result. Furthermore, the red-shift of the 253 nm band has been noticed for the CS-13 sample, indicating a decrease in copper oxide-substrate interaction[34,35].

H_2-Temperature programmed reduction (H_2-TPR) is a powerful tool to reveal the different types of copper oxide species on the catalysts. Figure 6 shows the H_2-TPR profile of the three samples prepared by using a different Cu^{2+}/NH_3 ratio. The main reduction peak (α_2), situated between 240 °C and 270 °C for all samples, is attributed to the reduction of well dispersed CuO [19,31]. The reduction signal at 600 °C (γ-peak) can be assigned to the reduction of Cu^+ to metallic copper. Its existence indicates that a small amount of CuO was firstly reduced to Cu^+ at a lower temperature, followed by its reduction to Cu^0 at 600 °C [38]. On the other hand, the small reduction shoulders on both sides of the main peak refer to CuO particles in weak interaction with the support (200 °C, α_1) and to poorly dispersed bulk CuO on the catalysts (300 °C, β), respectively [14][39]. As derived from TPR result, a poor CuO dispersion was achieved when the catalyst was prepared by the conventional wet impregnation method. This is evidenced by its high β-peak at a reduction temperature of 310 °C. On the contrary, all samples prepared by the ADP method contain mainly well-dispersed CuO while a small amount of bulk CuO and CuO loosely bonded on the support are also present. This result is in line with the aforementioned findings of N_2O pulse titration, XRD and UV-Vis-DR, suggesting the coexistence of several types of CuO species. When looking in more detail, a systematic shift of the main reduction peak can be observed from low to high Cu^{2+}/NH_3 ratio. A higher reduction temperature is associated with a higher energy requirement for the CuO reduction, which is directly correlated to a stronger metal-support interaction [8]. The latter finding further confirms the results derived from the UV-Vis-DR measurements. Hence, combining the results obtained by both techniques, it can be inferred that CuO present on the CS-16 sample exhibits a higher dispersion degree and stronger interaction with the silica support than the other two.

Figure 7 shows the representative TEM images of the samples. For the CS-13 and CS-14 (Figure 7 a, b), numerous large (10-20 nm) CuO particles can be observed, located outside the mesochannels, which is in line with the XRD and N_2O chemisorption results. On the contrary, CuO particles on the CS-16 sample are difficult to distinguish on the TEM image where only a few, small particles can be observed (Figure 7 c, d). This suggests the highly dispersed state (< 5 nm) of CuO on this material, as evidenced by the XRD, TPR and UV-Vis-DR analysis. The fact that large (10- 20 nm) CuO particles, as indicated by the N_2O titration, cannot be detected by TEM analysis suggests that bulk CuO is only present in a small percentage in CS-16 catalyst.

3.3 Thermal stability

For automotive application, particle migration and coalescence is the dominant particle growth mechanism for the copper oxide based catalysts, due to the elevated reaction temperature. In order to assess its influence on the CS-catalysts and correlate it to the materials' properties, the samples were exposed to a temperature of 700 °C for 6 hours.

ACCEPTED MANUSCRIPT

The representative X-ray diffractograms of the samples are shown in Figure 8. A significant increase in CuO crystallinity has been observed as a result of the increased particles' mobility, which accelerates particles' agglomeration. The same conclusion can be made based on the particles' size by the Scherrer equation, which reveals an enlargement of the CuO crystals (Table 4).

The XPS spectra of the thermally treated CuO/SBA-15 catalysts are displayed in Figure 9. After temperature treatment at 700°C, the $Cu2p_{3/2}$ peak at 935.9-936.1 eV decreases in intensity for all samples, referring to the particles migration and sintering. This hypothesis is further confirmed by the decrease in surface Cu/Si ratio summarized in Table 3. However, this phenomenon seems to be more limited on the CS-16 sample as it has the weakest decrease in the $Cu2p_{3/2}$ peak intensity and Cu/Si ratio after the thermal treatment.

Figure 10 illustrates the effect of thermal treatment on the reduction behavior of the catalysts, together with the relative percentage peak area summarized in Table 4. It can be seen that the elevated temperature gives rise to CuO aggregation on the silica surface, resulting in a higher percentage of bulk CuO. This phenomenon is most visible for CS-13 and CS-14, where respectively 76 % and 94 % of the total CuO loading is now present in the form of bulk CuO. On the other hand, the majority (about 56 %) of the well-dispersed CuO is preserved in CS-16 sample, pointing out its significant thermal stability in line with the XPS result. SEM analysis of CuO/SBA-15 catalysts before and after the heat treatment are illustrated in Figure 11. Before the thermal treatment, SEM images only reveal the typical mesoporous channels along the entire material with no visible CuO particles (Figure 11 a, c, e). In contrast, after exposure to 700 °C, large CuO particles become visible on the external surface of the supports (Figure 11 b, d, f). These large bulk CuO are sized between 0.5 to 1 µm in the case of CS-16 and are even larger for CS-13 and CS-14 sample (>5 µm). TEM images of the CS-16 sample (Figure 12) suggest that particle sizes below 5 nm still represent the majority of the Cu species, although larger particles could be spotted outside the materials' pores after the thermal treatment. Hence, it can be concluded that the high temperature treatment indeed accelerates the CuO migration and aggregation into larger particles, but the effect is limited for the CS-16 sample.

3.4 Catalytic performance

The impact of the divergent CuO dispersions on the catalytic activity, induced by the altered Cu^{2+}/NH_3 ratio during synthesis, was evaluated. The three catalysts were tested for their performance towards automotive exhaust gas conversion. Figure 13 demonstrates the pollutants' conversion as a function of the reaction temperature. The light-off temperature (temperature required for 50 % of reactant's conversion, T_{50}) and the maximum conversion (C_{max}) of each component are summarized in Table 5. As benchmark, a CuO/SBA-15 catalyst prepared by the conventional wet impregnation method (WI) with a similar wt.% in CuO was used (CS-WI).

Catalysts prepared by ADP method demonstrate an outstanding CO conversion capacity. The light-off temperature for CO conversion is 108 °C lower for the CS-16 than for the CS-WI sample. On the other hand, all three ADP samples reached the maximum CO conversion of 100 % from 230 °C while the C_{Max} is only 91 % for CS-WI. Secondly, the catalytic activity towards the hydrocarbons conversion also shows the benefit of the ADP method on the catalyst's performance. The maximum conversion of propane is only 10 % for the CS-WI sample, while a conversion of 100 % has been reached by all ADP samples. Finally, despite a decent propene C_{max} for the CS-WI (97 %), its light-off temperature is still about 200°C higher in comparison with the samples prepared by the ADP method. However, all copper oxide loaded catalysts possess a low CH_4 and NO conversion.

In addition, the catalytic activity of the copper oxide loaded samples was compared to that of a commercial precious metal loaded three-way catalyst (TWC). This catalyst has been crushed into

ACCEPTED MANUSCRIPT

powder with a similar grain size as the CuO loaded ones in order to exclude the heat and mass transfer differences. It can be seen that the CuO loaded catalysts prepared by the ADP method have a comparable activity with the TWC in the context of CO and hydrocarbons conversion. Furthermore, their T_{50} for the CO conversion is even lower (20 °C lower) than the commercial catalyst. However, the light-off temperature of propane and propene is much higher for the copper oxide loaded catalysts and the commercial vehicle exhaust catalyst also exhibits a superior NO conversion performance. Another remarkable finding that needs to be emphasized is the catalytic activity deviation among the ADP samples. Despite their comparable catalytic conversion towards various automotive pollutants, some small differences towards the catalytic selectivity can still be observed. It can be noticed that CS-14 sample has a slightly higher activity towards alkane conversion whilst CS-16 shows a remarkable performance for CO and C_3H_6. However, further tests are necessary in order to exclude the possible experimental error within the results (about 5% for both the temperature registration and quantitative measurements).

Overall, the catalytic test result indicates the great efficiency of the ADP method in preparing a highly dispersed CuO catalyst which has the potential for automotive oxidation reactions. However, an important aspect that still needs to be discussed regarding the catalytic performance of the materials is the addition of catalytic promoters. The modern TWC consists of several catalytic promoters or co-catalysts such as ZrO_2 and CeO_2 for improving the materials activity and lifespan [40]. Evidently, these promoters are not present in our synthesized copper oxide loaded samples, meaning that their catalytic activity can be further improved by selection and addition of a suitable promoter or co-catalyst in the near future.

An important focus of this investigation is the influence of the Cu^{2+}/NH_3 ratio on the catalyst's life span. For this reason, the catalytic activity of the CS-16 sample has been monitored at 700 °C for 8 hours (Figure 14). The CuO/SBA-15 prepared by the conventional wet impregnation method has also been subjected to the life-span test as benchmark. During a time-on-stream of 8 hours, a preservation of CO, C_3H_6 and C_3H_8 conversion can be observed for the CS-16 sample while a significant decline of CH_4 and NO conversion is observed in function of the time-on-stream. On the contrary, the sample prepared by the WI method demonstrates a strong decrease of its overall catalytic performance already after two hours of time-on-stream with the exception of propene conversion that remains constant. The result of catalytic life-span test again confirmed the beneficial effect of the ADP method towards thermal and catalyst stability, when using a Cu^{2+}/NH_3 of 1/6 of the CuO-loaded catalyst.

4. Discussion

4.1 The formation of grafted copper oxide and phyllosilicate

It is known that during the metal impregnation based on NH_3 addition, the Cu^{2+} ions interact with NH_3 and H_2O within the solution in order to form the positively charged $[Cu(NH_3)_4(H_2O)_2]^{2+}$ complex. This complex interacts electrostatically with two negatively charged surface silanol groups created by the high pH solution [16]. At the same time, the formation of a copper hydroxide complex $(Cu(OH)_2(H_2O)_4)$ occurs, which is in competition with the copper-ammonia complex formation (Equation 2) [20].

$$[\mathrm{Cu(NH_3)_4(H_2O)_2}]^{2+} + 2\mathrm{OH^-} + 2\mathrm{H_2O} \leftrightarrow \mathrm{Cu(OH)_2(H_2O)_4} + 4\mathrm{NH_3} \qquad \text{Equation 2}$$

During the sample drying, the copper-ammonia complex interacting with the surface undergoes an ion-exchange process where two NH_3 ligands of the copper tetra-ammonia complex are replaced by

ACCEPTED MANUSCRIPT

two ≡SiO$^-$ ligands. This leads to the formation of the so-called grafted CuO (≡Si-O-Cu), which is also known as ion-exchanged Cu-O-Si (Equation 3):

$$[\mathrm{Cu(NH_3)_4(H_2O)_2}]^{2+} + 2[\equiv SiO]^- \rightarrow$$

$$(\equiv \mathrm{SiO})_2\mathrm{Cu(NH_3)_2(H_2O)_2} + 2\ \mathrm{NH_3} \rightarrow \equiv Si - O - Cu\ \ (\text{Grafted CuO}) \qquad \text{Equation 3}$$

Meanwhile, the zero charged $Cu(OH)_2(H_2O)_4$ complex reacts with the silicic acid ($Si(OH)_4$) dissolved from the surface silica to yield copper phyllosilicate (Equation 4) [18].

$$\mathrm{Si(OH)_4} + \mathrm{Cu(OH)_2(H_2O)_4} \rightarrow \text{Copper phyllosilicate} \qquad \text{Equation 4}$$

Nevertheless, no proof for the presence of phyllosilicate could be found in the prepared catalyst materials.

4.2 The influence of NH_3

Within this investigation, we systematically increased the molar Cu^{2+}/NH_3 ratio during the synthesis while the other synthesis parameters were kept constant. By doing so, a positive trend has been observed regarding the catalyst's CuO dispersion and thermal stability. Here, it is important to point out that despite the same pH value for all three samples, their absolute amount of NH_3 is different. While the solutions' pH is determined by the concentration of NH_3, the absolute NH_3 amount is controlled by the total added NH_3 during the synthesis, which is in our case based on the molar Cu^{2+}/NH_3 ratio. This important feature differentiates the methodological approach of our investigation from the other existing research in the field of ammonia based impregnation in which both pH and thus OH^- concentration and Cu^{2+}/NH_3 ratio is varied. During the metal impregnation, the higher NH_3 amount on the CS-16 samples will shift the equilibrium in favor of the copper tetra-ammonia complex formation (Equation 2, left). Consequently, the CuO formation will mainly occur according to Equation 3. After sample calcination at 550 °C, the copper ammonia complex that strongly interacted with the support will transform into grafted CuO. On the other hand, the insufficient amount of ammonia for CS-13 leads to more zero charged $Cu(OH)_2(H_2O)_4$. However, one could wonder why there is no phyllosilicate observed in the DRIFT analysis of this sample. The reason behind this lies in the absolute amount of OH^- ions, which is the crucial reactant for the silicic acid ($Si(OH)_4$) formation. The OH^- is formed during the autoprotolysis of water in the basic medium. In our case, this basic pH is brought by the addition of ammonia. However, at the same time, the ammonia present in the solution has also been consumed for the copper tetra-ammine complex formation. Because of the ammonia requirement from both the copper complex and silicic acid formation, a shortage of ammonia (especially for CS-13) will lead to a lower amount of OH^- ions within the solution and consequently suppresses the silicic acid formation. This hypothesis is supported by N_2-sorption data of the samples, which points out a significant lower pore enlargement for the CS-13 sample as a result of limited silica's outer layer dissolution (Table 2). For this reason, the formed zero charged $Cu(OH)_2(H_2O)_4$ will not react with the silicic acid to form phyllosilicate. Instead, it will transform into a well-dispersed CuO layer over the grafted CuO or to bulk CuO with a larger particle size.

The above postulated mechanism is in line with the conclusion derived from the TPR profile, which suggests the presence of three types of CuO species for all samples, namely well-dispersed CuO loosely bonded onto the support, grafted CuO grafted on the support and a small amount of bulk CuO. Furthermore, the shift of the major reduction peak for CS-16 to a higher temperature can also be explained since CS-16 mainly possesses grafted CuO. Besides the strong metal support interaction, CuO particles present on the CS-16 have a slightly smaller average particle size, as concluded from the XRD analysis. The latter observation is consistent with literature, indicating that a stronger metal-support

ACCEPTED MANUSCRIPT

interaction yields smaller metal particles on the catalysts due to the suppressed particles' mobility and sintering prevention during calcination [11]. Herein, the dilution effect on the CuO dispersion needs also be considered since a higher CuO concentration will cause a local concentration gradient during the impregnation, leading to a inhomogeneous CuO dispersion [13]. This effect is more profound for CS-13 since it has the highest Cu concentration. However, this dilution effect does not explain the formation of highly support interacting metal particles.

4.3 Structure-activity and -stability relationships

According to the catalytic test results, catalysts prepared by the ADP approach have a promising activity towards the automotive emission control in the context of CO and hydrocarbons conversion. Furthermore, their activity is even comparable with the commercial precious metal loaded three-way catalyst. The excellent catalytic activity of the ADP samples is mainly a result of a high CuO dispersion brought by the well-designed impregnation method. The strong influence of the metal dispersion on the final catalytic activity is more prominent when we compared the result with the same catalyst prepared by the conventional wet impregnation method. It is known that the latter approach often results in a dominant presence of a bulk CuO phase. In our case, this poor CuO dispersion indeed leads to a significant lower catalytic activity.

As mentioned before, when comparing the catalysts synthesized by a different Cu^{2+}/NH_3 ratio, one can clearly observe the slight differences between the samples regarding their catalytic oxidation activity. This deviation in activity can not solely result from the CuO dispersion because a comparable dispersion degree among these samples has been determined, especially for the CS-14 and CS-16 sample. As evidenced by the UV-Vis-DR, XPS and H_2-TPR, several types of well-dispersed CuO species with divergent properties were distinguished. Hence, besides the CuO dispersion, the type, size and coordination of the CuO species also play a crucial role in the materials' activity and in particular the catalytic selectivity. However, although clear differences can be observed in TPR and UV-vis-DR, it is difficult to prove a solid correlation between those factors and the catalytic selectivity as the different CuO species among the mutual samples and their catalytic activity is negligible. Nevertheless, this latter observation is worthy of future attention and further investigation.

Apart from the deviation in the structure-activity relationship between the synthesized materials, the main finding of this work is the enhanced catalytic life-span brought by a higher Cu^{2+}/NH_3 molar ratio despite the comparable CuO dispersion. The dominant presence of the grafted CuO on the CS-16 yields a significant improvement on the material's thermal stability, as confirmed by its XRD, H_2-TPR and TEM. The strong metal-support interaction provided by the grafted CuO probably limits the particles' mobility at a high temperature, which suppresses the metal sintering phenomenon. This observation is further supported by its catalytic durability test in function of time-on-stream. CuO/SBA-15 prepared with a 1/6 Cu^{2+}/NH_3 ratio demonstrates a preservation of its excellent activity after a run time of 8 hours while a strong decline of the activity has been observed for the WI sample.

5. Conclusion

The present work demonstrated the potential of CuO as the active element for the automotive oxidation catalyst by applying a modified ammonia driven deposition precipitation. CuO/SBA-15 catalysts prepared by this method exhibit isolated CuO with a strong support interaction as the dominant copper species on the support. This excellent copper oxide dispersion has been translated into a promising automotive oxidation performance, which is even comparable with that of the current industrial precious metal based three-way catalyst in terms of conversion and light-off temperature. Unfortunately, the NO conversion is much less.

ACCEPTED MANUSCRIPT

When a higher molar Cu^{2+}/NH_3 ratio of 1/6 has been applied, a dominant grafted CuO phase has been observed together with a smaller fraction of bulk CuO, compared to lower Cu^{2+}/NH_3 ratios and the classical wet impregnation method. This type of CuO phase is in strong interaction with the support, leading to an enhanced catalyst's thermal stability and life span due to the suppression of metal particles' mobility. Herein, the dispersion and interaction between Cu^{2+} ions and the support surface plays a key role. Finally, it is important to mention that this catalyst preparation method can also be implemented on copper oxide-loaded catalysts for other applications, in which the CuO dispersion and support interaction in combination with thermal stability is of utmost importance.

6. Acknowledgement

The authors kindly acknowledge Johnson Matthey for providing the commercial precious metal loaded three-way catalyst.

7. Funding

This work was supported by EU-FP 7: Next-Gen-Cat project [grant agreement number: 280890].

8. References

[1] F.E. López-Suárez, a. Bueno-López, M.J. Illán-Gómez., Cu/Al_2O_3 catalysts for soot oxidation: Copper loading effect, Appl. Catal. B Environ. 84 (2008) 651–658. doi:10.1016/j.apcatb.2008.05.019.

[2] Z. Huang, F. Cui, H. Kang, J. Chen, C. Xia, Characterization and catalytic properties of the CuO/SiO_2 catalysts prepared by precipitation-gel method in the hydrogenolysis of glycerol to 1,2-propanediol: Effect of residual sodium, Appl. Catal. A Gen. 366 (2009) 288–298. doi:10.1016/j.apcata.2009.07.017.

[3] Y.Y. Zhu, S.R. Wang, L.J. Zhu, X.L. Ge, X.B. Li, Z.Y. Luo, The Influence of Copper Particle Dispersion in Cu/SiO_2 Catalysts on the Hydrogenation Synthesis of Ethylene Glycol, Catal. Letters. 135 (2010) 275–281. doi:10.1007/s10562-010-0298-z.

[4] J.T. Kummer, Catalysts for automobile emission control, Prog. Energy Combust. Sci. 6 (1982) 177. doi:10.1016/0360-1285(80)90006-4.

[5] I. Fechete, Y. Wang, J.C. Védrine, The past, present and future of heterogeneous catalysis, Catal. Today. 189 (2012) 2–27. doi:10.1016/j.cattod.2012.04.003.

[6] A. Jos van Dillen, R. Terorde, D.J. Lensveld, J.W. Geus, K.P. de Jong, Synthesis of supported catalysts by impregnation and drying using aqueous chelated metal complexes, J. Catal. 216 (2003) 257–264. doi:10.1016/S0021-9517(02)00130-6.

[7] M. V. Twigg, M.S. Spencer, Deactivation of supported copper metal catalysts for hydrogenation reactions, Appl. Catal. A Gen. 212 (2001) 161–174. doi:10.1016/S0926-860X(00)00854-1.

[8] R. van den Berg, T.E. Parmentier, C.F. Elkjær, C.J. Gommes, J. Sehested, S. Helveg, et al., Support Functionalization To Retard Ostwald Ripening in Copper Methanol Synthesis Catalysts, ACS Catal. 5 (2015) 4439–4448. doi:10.1021/acscatal.5b00833.

[9] T.W. Hansen, A.T. Delariva, S.R. Challa, A.K. Datye, Sintering of catalytic nanoparticles: Particle

ACCEPTED MANUSCRIPT

migration or ostwald ripening?, Acc. Chem. Res. 46 (2013). doi:10.1021/ar3002427.

[10] G. Prieto, J. Zečević, H. Friedrich, K.P. de Jong, P.E. de Jongh, Towards stable catalysts by controlling collective properties of supported metal nanoparticles., Nat. Mater. 12 (2013) 34–9. doi:10.1038/nmat3471.

[11] J.A. Farmer, C.T. Campbell, Ceria maintains smaller metal catalyst particles by strong metal-support bonding, Science 329 (2010) 933–936. doi:10.1126/science.1191778.

[12] J. Matthey, Forecast of Platinum Supply & Demands in 2014, (2014) 1–32. www.platinum.matthey.com/documents/new-item/pgm%20market%20reports/pgm%20market%20report%20november%202015.pdf&usg=AFQjCNFcHLV5hPhuFOyFS2G7l19nhZEWBA&sig2=ZjbjI1fYY11VzQXbAezbNg&cad=rja.

[13] P. Munnik, P.E. de Jongh, K.P. de Jong, Recent Developments in the Synthesis of Supported Catalysts., Chem. Rev. 115 (2015) 6687–6718. doi:10.1021/cr500486u.

[14] L. Chen, P. Guo, M. Qiao, S. Yan, H. Li, W. Shen, et al., Cu/SiO_2 catalysts prepared by the ammonia-evaporation method: Texture, structure, and catalytic performance in hydrogenation of dimethyl oxalate to ethylene glycol, J. Catal. 257 (2008) 172–180. doi:10.1016/j.jcat.2008.04.021.

[15] A. García-Trenco, A. Martínez, A simple and efficient approach to confine Cu/ZnO methanol synthesis catalysts in the ordered mesoporous SBA-15 silica, Catal. Today. 215 (2013) 152–161. doi:10.1016/j.cattod.2013.03.005.

[16] L. Trouillet, T. Toupance, Ó. Villain, C. Louis, D. Re, U.M.R. Cnrs, et al., In situ characterization of the coordination sphere of Cu II complexes supported on silica during the preparation of Cu/SiO_2 catalysts by cation exchange, Phys. Chem. Chem. Phys. 2 (2000) 2005–2014. doi:10.1039/a909427j.

[17] T. Toupance, M. Kermarec, C. Louis, Metal Particle Size in Silica-Supported Copper Catalysts. Influence of the Conditions of Preparation and of Thermal Pretreatments, J. Phys. Chem. B. 104 (2000) 965–972. doi:10.1021/jp993399q.

[18] T. Toupance, M. Kermarec, C. Louis, Conditions of Formation of Copper Phyllosilicates in Silica-Supported Copper Catalysts Prepared by Selective Adsorption, J. Phys. Chem. B. 106 (2002) 2277–2286. doi:10.1021/jp013153x.

[19] B. Zhang, S. Hui, S. Zhang, Y. Ji, W. Li, D. Fang, Effect of copper loading on texture, structure and catalytic performance of Cu/SiO_2 catalyst for hydrogenation of dimethyl oxalate to ethylene glycol, J. Nat. Gas Chem. 21 (2012) 563–570. doi:10.1016/S1003-9953(11)60405-2.

[20] S. Zhu, X. Gao, Y. Zhu, W. Fan, J. Wang, Y. Li, Highly efficient and robust Cu/SiO_2 catalyst prepared by the ammonia evaporation hydrothermal method for glycerol hydrogenolysis to 1,2-propanediol., Catal. Sci. Technol. 5 (2015) 1169–1180. doi:10.1039/C4CY01148A.

[21] H. Yue, Y. Zhao, S. Zhao, B. Wang, X. Ma, J. Gong, A copper-phyllosilicate core-sheath nanoreactor for carbon-oxygen hydrogenolysis reactions., Nat. Commun. 4 (2013) 2339. doi:10.1038/ncomms3339.

[22] Q. Xin, A. Glisenti, C. Philippopoulos, E. Poulakis, M. Mertens, J. Nyalosaso, et al., Comparison between a Water-Based and a Solvent-Based Impregnation Method towards Dispersed CuO/SBA-15 Catalysts: Texture, Structure and Catalytic Performance in Automotive Exhaust Gas Abatement, Catalysts. 6 (2016) 164. doi:10.3390/catal6100164.

[23] X. Guo, A. Yin, W.-L. Dai, K. Fan, One Pot Synthesis of Ultra-High Copper Contented Cu/SBA-15

ACCEPTED MANUSCRIPT

Material as Excellent Catalyst in the Hydrogenation of Dimethyl Oxalate to Ethylene Glycol, Catal. Letters. 132 (2009) 22–27. doi:10.1007/s10562-009-0043-7.

[24] V. Meynen, P. Cool, E.F. Vansant, Verified syntheses of mesoporous materials, Microporous Mesoporous Mater. 125 (2009) 170–223. doi:10.1016/j.micromeso.2009.03.046.

[25] M.J. Luys, P.H. Van Oeffelt, W.G.J. Brouwer, A.P. Pijpers, J.J.F. Sscholten, Surface and sub-surface oxidation of copper and supported copper catalysts by nitrous oxide, Appl. Catal. 46 (1989) 161–173. doi:10.1016/S0166-9834(00)81401-3.

[26] G. Smeulders, V. Meynen, A. Silvestre-Albero, K. Houthoofd, M. Mertens, J. Silvestre-Albero, et al., The impact of framework organic functional groups on the hydrophobicity and overall stability of mesoporous silica materials, Mater. Chem. Phys. 132 (2012) 1077–1088. doi:10.1016/j.matchemphys.2011.12.072.

[27] M. Thommes, K. Kaneko, A. V. Neimark, J.P. Olivier, F. Rodriguez-Reinoso, J. Rouquerol, et al., Physisorption of gases, with special reference to the evaluation of surface area and pore size distribution (IUPAC Technical Report), Pure Appl. Chem. 87 (2015) 1051–1069. doi:10.1515/pac-2014-1117.

[28] G. Prieto, M. Shakeri, K.P. de Jong, P.E. de Jongh, Quantitative Relationship between Support Porosity and the Stability of Pore-Confined Metal Nanoparticles Studied on $CuZnO/SiO_2$ Methanol Synthesis Catalysts., ACS Nano. 8 (2014) 2522–2531. doi:10.1021/nn406119j.

[29] F. Li, C.-S. Lu, X.-N. Li, The effect of the amount of ammonia on the Cu^0/Cu^+ ratio of Cu/SiO_2 catalyst for the hydrogenation of dimethyl oxalate to ethylene glycol, Chinese Chem. Lett. 25 (2014) 1461–1465. doi:10.1016/j.cclet.2014.05.050.

[30] A. Yin, X. Guo, W.L. Dai, K. Fan, The nature of active copper species in cu-hms catalyst for hydrogenation of dimethyl oxalate to ethylene glycol: New insights on the synergetic effect between Cu^0 and Cu^+, J. Phys. Chem. C. 113 (2009) 11003–11013. doi:10.1021/jp902688b.

[31] Z. Huang, F. Cui, J. Xue, J. Zuo, J. Chen, C. Xia, Cu/SiO_2 catalysts prepared by hom- and heterogeneous deposition–precipitation methods: Texture, structure, and catalytic performance in the hydrogenolysis of glycerol to 1,2-propanediol, Catal. Today. 183 (2012) 42–51. doi:10.1016/j.cattod.2011.08.038.

[32] R. Zhang, D. Shi, Y. Zhao, B. Chen, J. Xue, X. Liang, et al., The reaction of $NO+C_3H_6+O_2$ over the mesoporous SBA-15 supported transition metal catalysts, Catal. Today. 175 (2011) 26–33. doi:10.1016/j.cattod.2011.04.014.

[33] J. Batista, A. Pintar, D. Mandrino, M. Jenko, V. Martin, XPS and TPR examinations of γ-alumina-supported Pd-Cu catalysts, Appl. Catal. A Gen. 206 (2001) 113–124. doi:10.1016/S0926-860X(00)00589-5.

[34] A.T. Shah, B. Li, Z.E.A. Abdalla, Direct synthesis of Cu-SBA-16 by internal pH-modification method and its performance for adsorption of dibenzothiophene, Microporous Mesoporous Mater. 130 (2010) 248–254. doi:10.1016/j.micromeso.2009.11.017.

[35] J. Escobar, J.A. De Los Reyes, T. Viveros, Nickel on TiO_2-modified Al_2O_3 sol-gel oxides: Effect of synthesis parameters on the supported phase properties, Appl. Catal. A Gen. 253 (2003) 151–163. doi:10.1016/S0926-860X(03)00501-5.

[36] P. Kuśtrowski, L. Chmielarz, R. Dziembaj, P. Cool, E.F. Vansant, Modification of MCM-48-, SBA-15-, MCF-, and MSU-type mesoporous silicas with transition metal oxides using the molecular designed dispersion method., J. Phys. Chem. B. 109 (2005) 11552–8. doi:10.1021/jp050696o.

ACCEPTED MANUSCRIPT

[37] H. Praliaud, S. Mikhailenko, Z. Chajar, M. Primet, Surface and bulk properties of Cu-ZSM-5 and Cu/Al2O3 solids during redox treatments. Correlation with the selective reduction of nitric oxide by hydrocarbons, Appl. Catal. B Environ. 16 (1998) 359–374. doi:10.1016/S0926-3373(97)00093-3.

[38] C.J.G. Van Der Grift, P.A. Elberse, A. Mulder, J.W. Geus, Preparation of Silica-Supported Copper Catalysts by means of Deposition-Precipitation, Appl. Catal. 59 (1990) 275–289. doi:10.1016/S0166-9834(00)82204-6.

[39] A.J. Marchi, Dehydrogenation of isopropylic alcohol on a Cu/SiO_2 catalyst: a study of the activity evolution and reactivation of the catalyst, Appl. Catal. A Gen. 142 (1996) 375–386. doi:10.1016/0926-860X(96)00087-7.

[40] C.H. Bartholonew, R.J. Farrauto, Fundamentals of Industrial Catalytic Processes, 2nd Ed., Wiley-Interscience, Hoboken, New Jersey, 2005.

ACCEPTED MANUSCRIPT

Figure captions

Fig. 1: N_2-physisorption isotherms of a) SBA-15 and CuO/SBA-15 catalysts prepared with b) 1/3, c) 1/4 and d) 1/6 molar Cu^{2+}/NH_3 ratio after calcination at 550 °C.

Fig. 2: Vacuum-DRIFT spectra of a) SBA-15 and uncalcined b) CS-13, c) CS-14, d) CS-16.

Fig. 3: X-ray diffraction patterns of the CuO/SBA-15 materials prepared with different Cu^{2+}/NH_3 molar ratio after calcination at 550 °C, together with the same catalyst prepared by WI method.

Fig. 4: XPS spectra of $Cu2p_{3/2}$ region of the CuO/SBA-15 materials prepared with different Cu^{2+}/NH_3 molar ratio after calcination at 550 °C, together with the same catalyst prepared by WI method.

Fig. 5: UV-Vis-DR spectra of the CuO/SBA-15 materials prepared with different Cu^{2+}/NH_3 molar ratio after calcination at 550 °C.

Fig. 6: Normalized H_2-TPR profiles of the CuO/SBA-15 materials prepared with different Cu^{2+}/NH_3 molar ratio after calcination at 550 °C, together with the same catalyst prepared by WI method.

Fig. 7: TEM image of CuO/SBA-15 catalysts prepared with a) 1/3, b) 1/4 and c,d) 1/6 molar Cu^{2+}/NH_3 ratio after calcination at 550 °C.

Fig. 8: X-ray diffraction patterns of the CuO/SBA-15 materials prepared with different Cu^{2+}/NH_3 molar ratio after calcination and after heat treatment at 700 °C.

Fig. 9: XPS spectra of $Cu2p_{3/2}$ region of the CuO/SBA-15 materials prepared with different Cu^{2+}/NH_3 molar ratio after calcination and after heat treatment at 700 °C.

Fig. 10: Normalized H_2-TPR profiles of the CuO/SBA-15 materials prepared with different Cu^{2+}/NH_3 molar ratio after calcination and after heat treatment at 700 °C.

Fig. 11: SEM images of CuO/SBA-15 prepared by a Cu^{2+}/NH_3 molar ratio of a) 1/3 after calcination at 550 °C, b) 1/3 after heat treatment of 700 °C, c) 1/4 after calcination at 550 °C, d) 1/4 after heat treatment of 700 °C, e) 1/6 after calcination at 550 °C, f) 1/6 after heat treatment of 700 °C.

Fig. 12 a, b: TEM images of CuO/SBA-15 prepared with 1/6 molar Cu^{2+}/NH_3 ratio after heat treatment of 700 °C.

Fig. 13: Catalytic performance under stoichiometric condition of commercial three-way catalyst (TWC) and CuO/SBA-15 catalysts prepared by wet impregnation method (CS-WI) and ADP method with different Cu^{2+}/NH_3 ratio for a) CO, b) CH_4, c) C_3H_6, d) C_3H_8 and e) NO conversion.

Figure 14: Catalytic performance under stoichiometric condition of a) CS-WI and b) CS-16 catalyst as a function of time-on stream. (●: CO, ▲: CH_4, ▼: C_3H_6, ♦: C_3H_8, ■: NO)

Figure 1

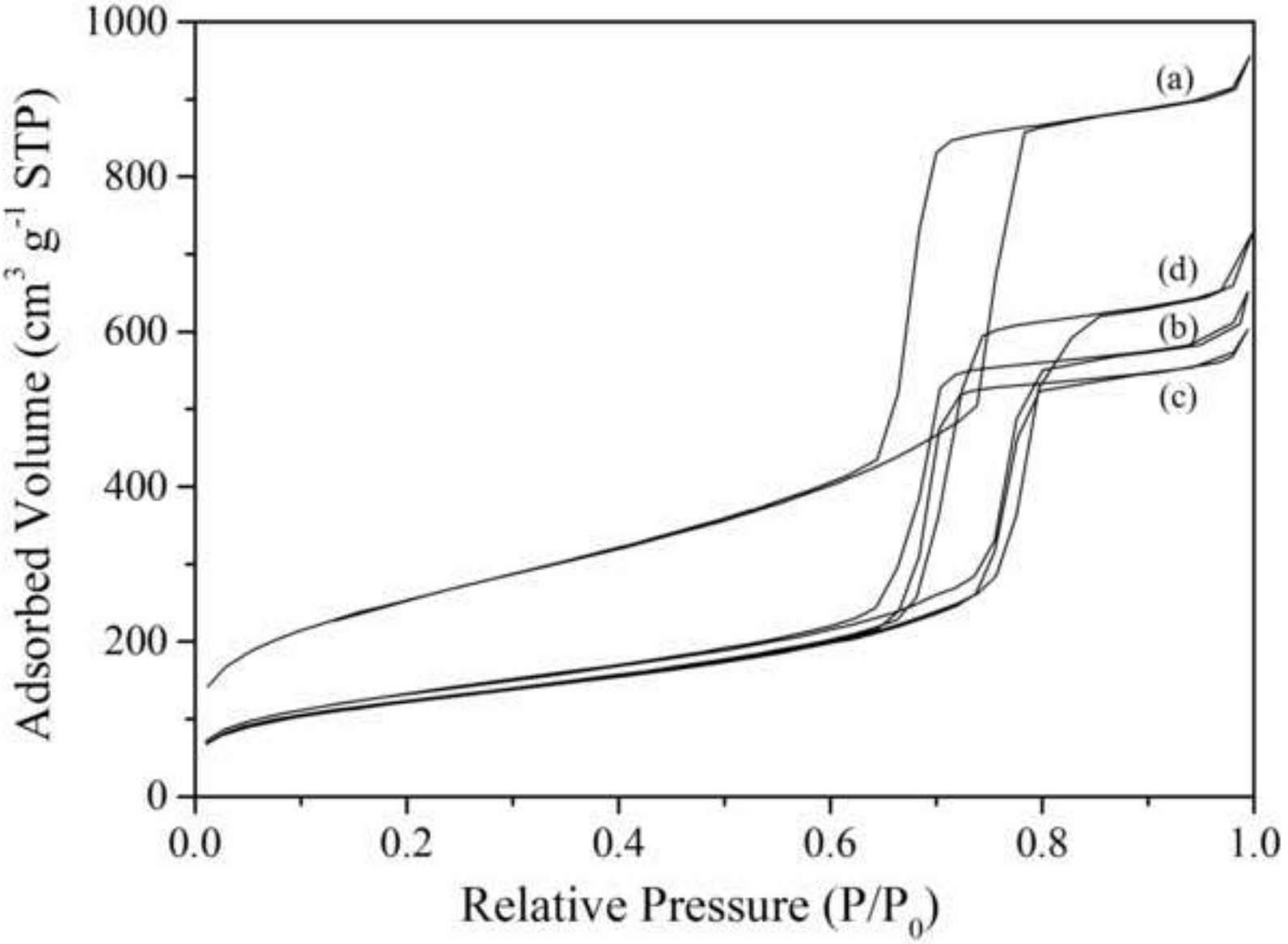
1000
800
600
400
200
0
0.0
0.2
0.4
0.6
0.8
1.0
Adsorbed Volume (cm^3 g^{-1} STP)
Relative Pressure (P/P$_0$)
(a)
(d)
(b)
(c)

Figure 2

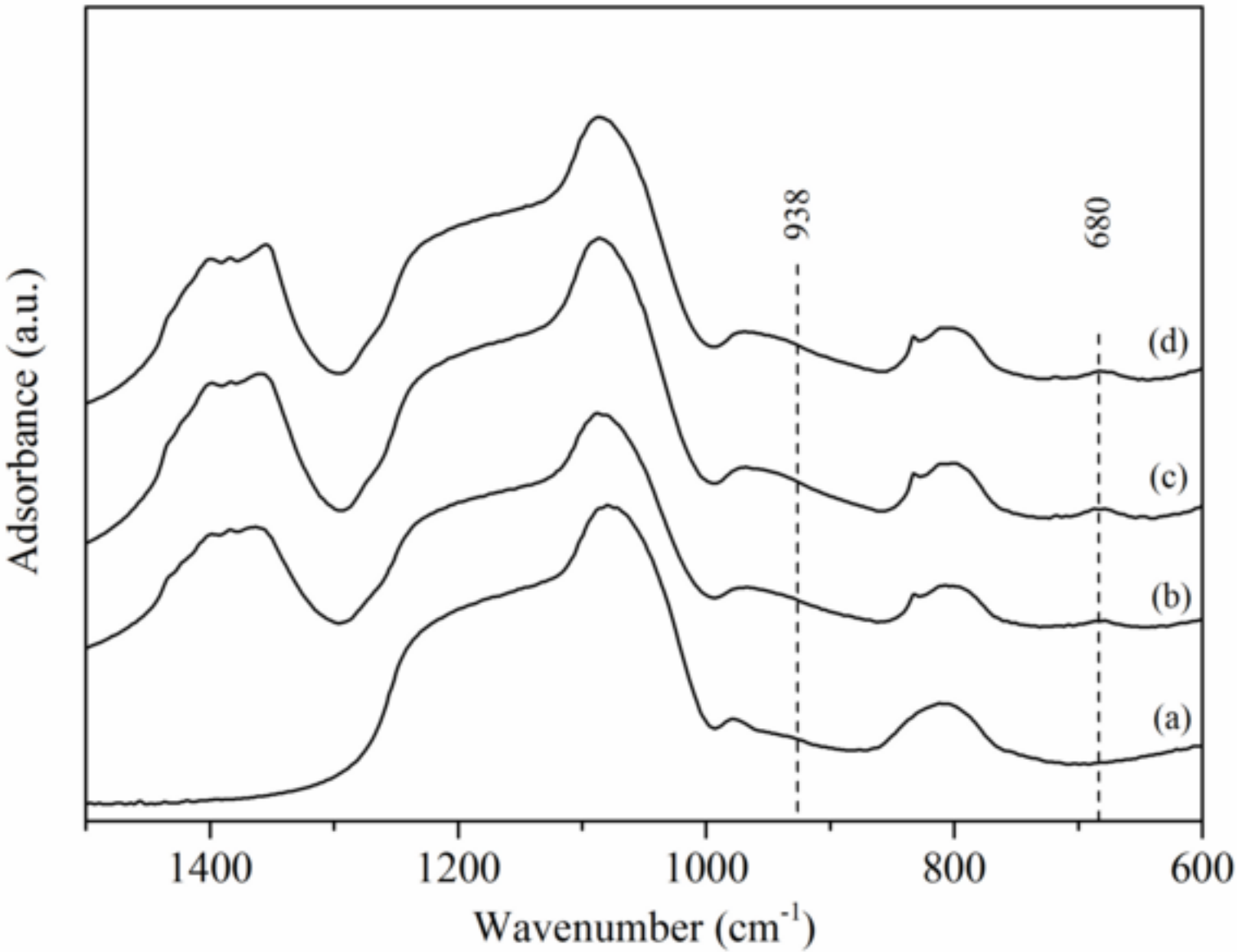
Adsorbance (a.u.)
938
680
(d)
(c)
(b)
(a)
1400
1200
1000
800
600
Wavenumber (cm-1)

Figure 3

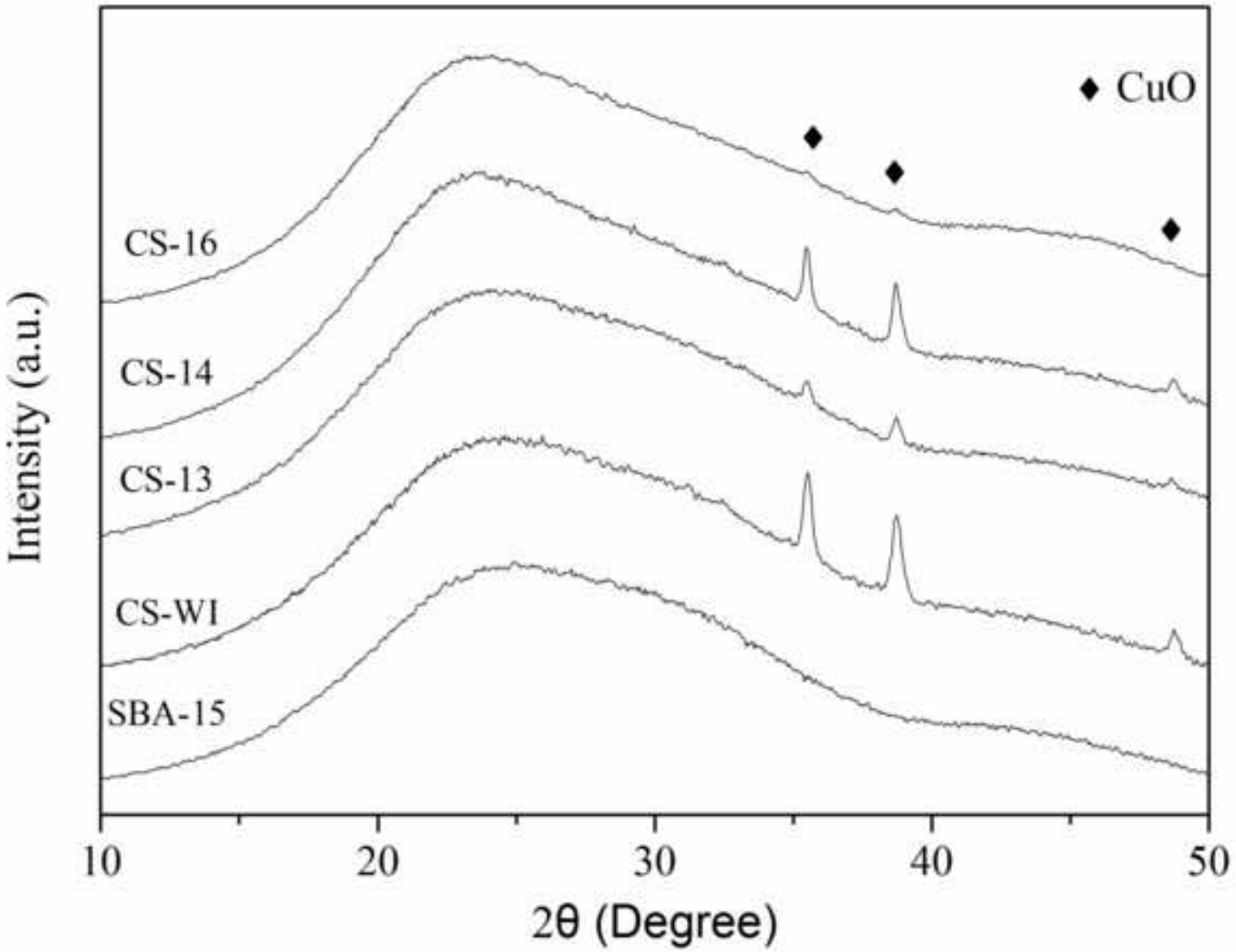
◆ CuO
CS-16
CS-14
CS-13
CS-WI
SBA-15
Intensity (a.u.)
10
20
30
40
50
2θ (Degree)

Figure 4

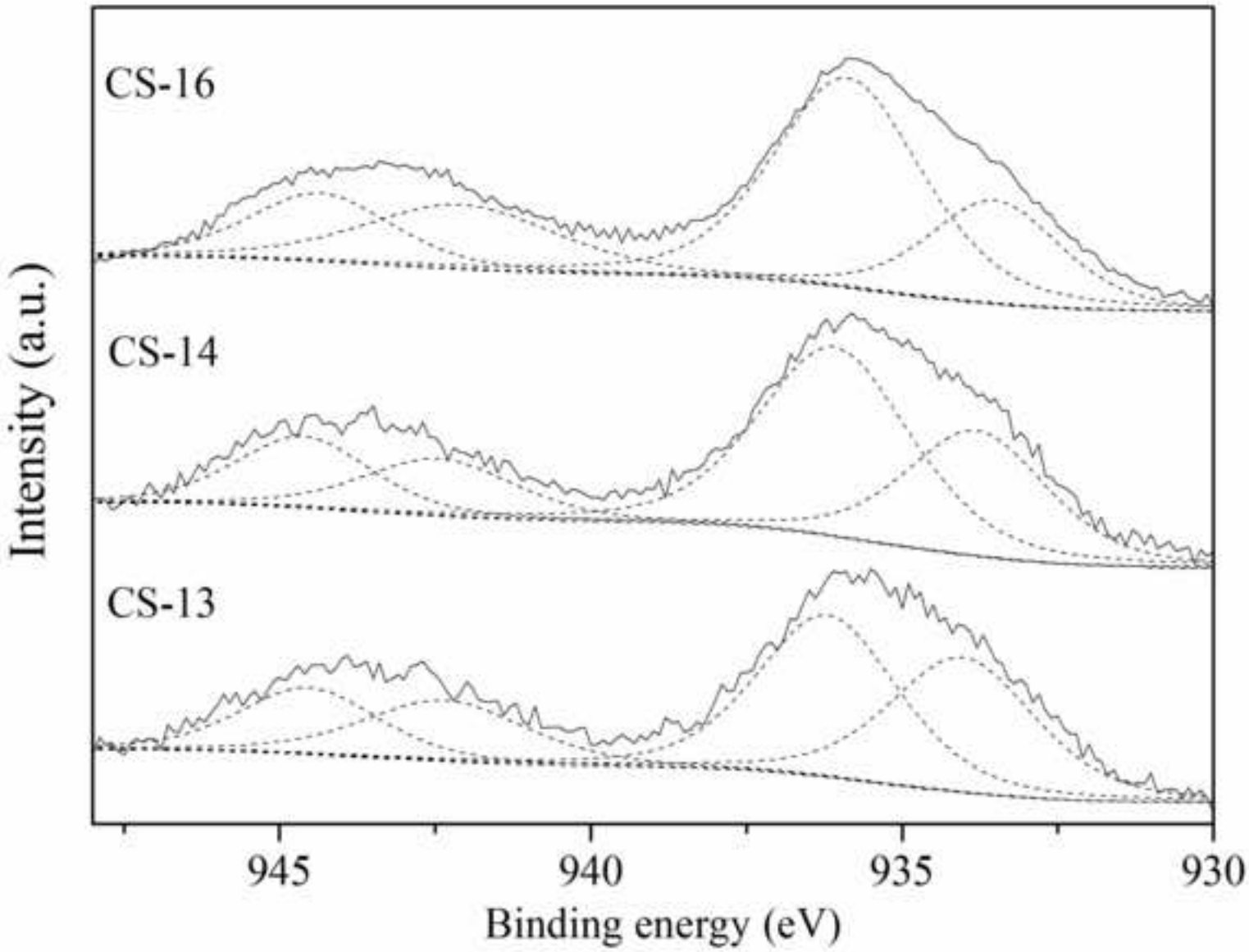
CS-16
CS-14
CS-13
Intensity (a.u.)
945
940
935
930
Binding energy (eV)

Figure 5

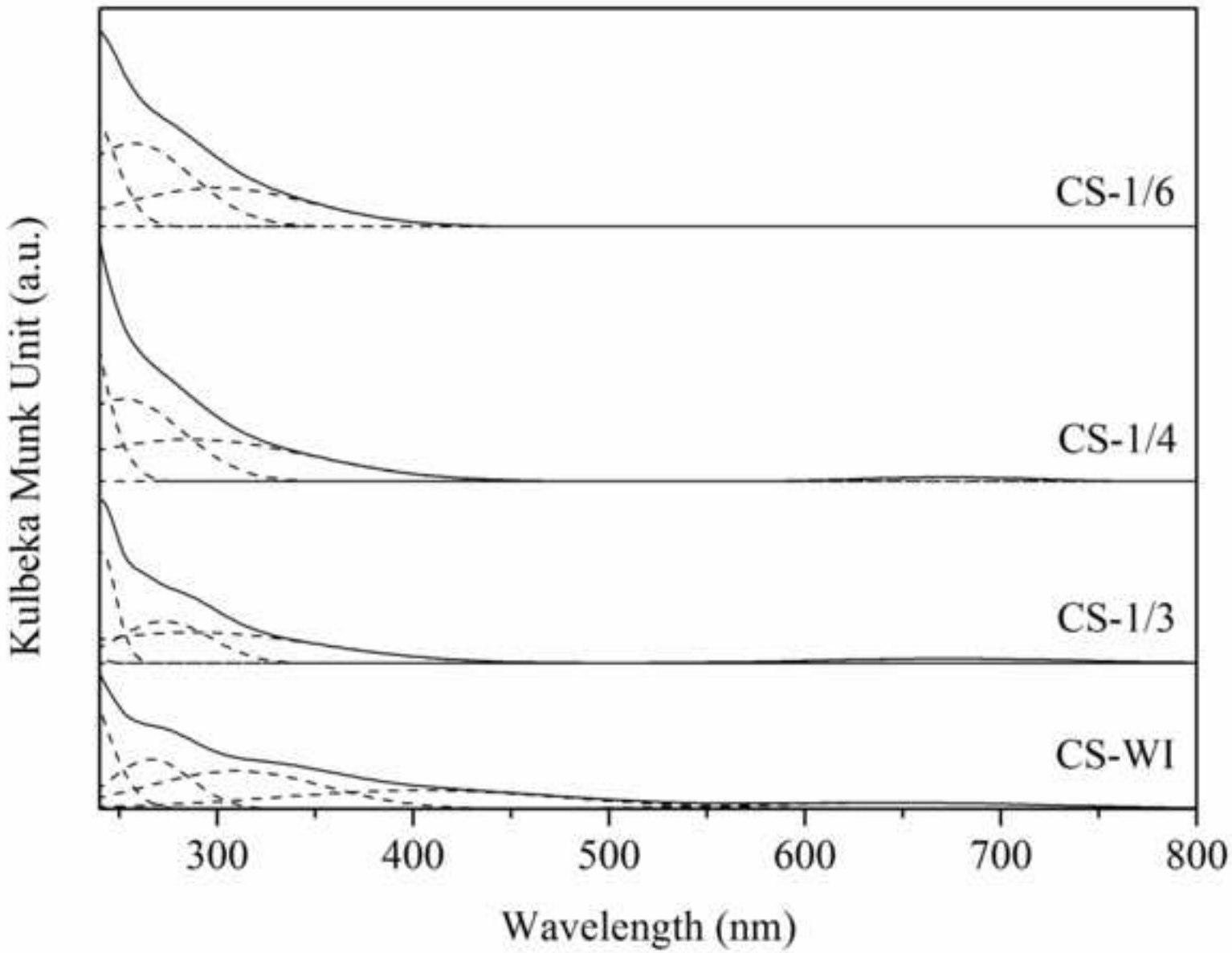
Kulbeka Munk Unit (a.u.)
CS-1/6
CS-1/4
CS-1/3
CS-WI
300
400
500
600
700
800
Wavelength (nm)

Figure 6

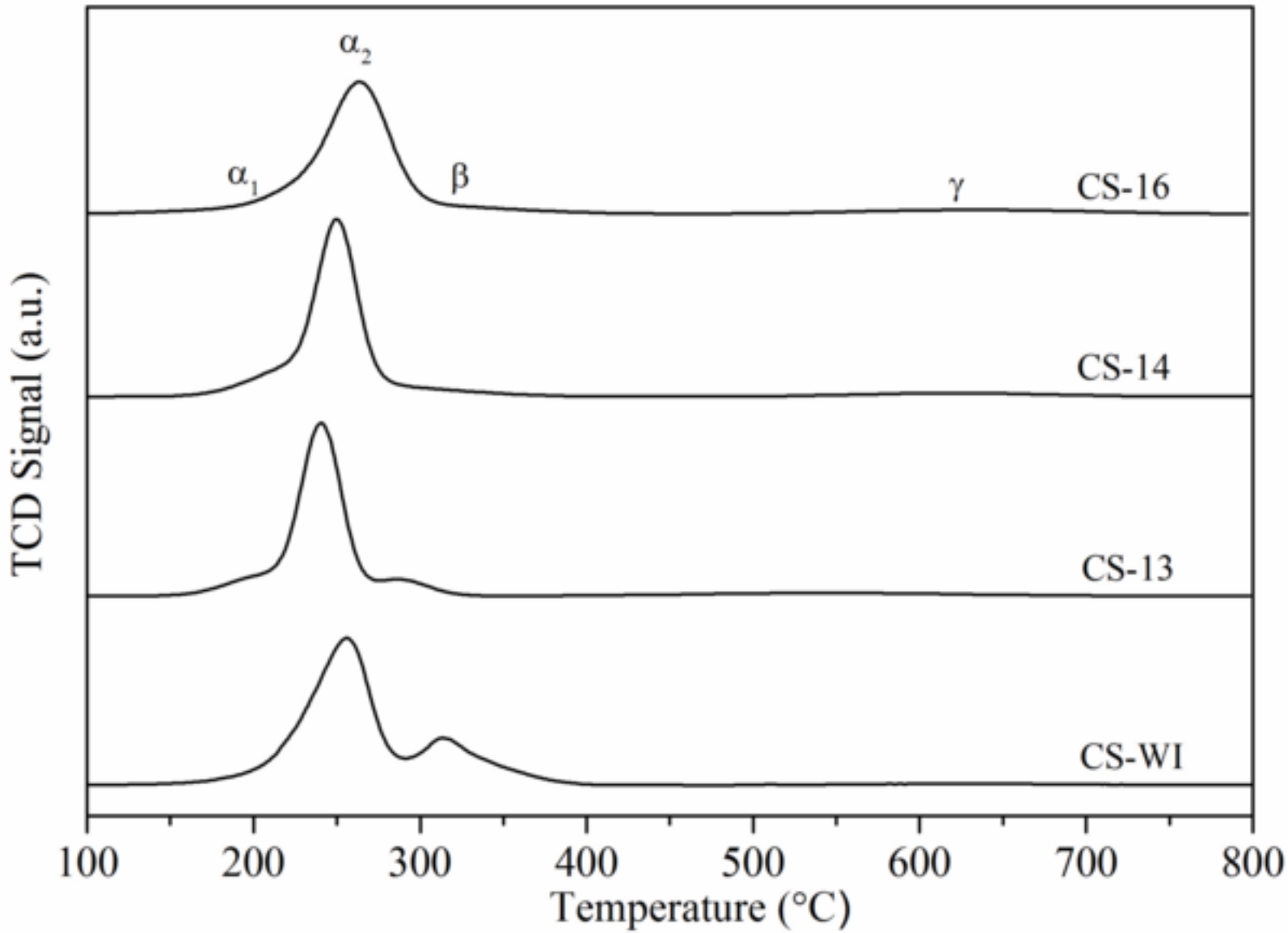
α2
α1
β
γ
CS-16
CS-14
CS-13
CS-WI
TCD Signal (a.u.)
100
200
300
400
500
600
700
800
Temperature (°C)

Figure7

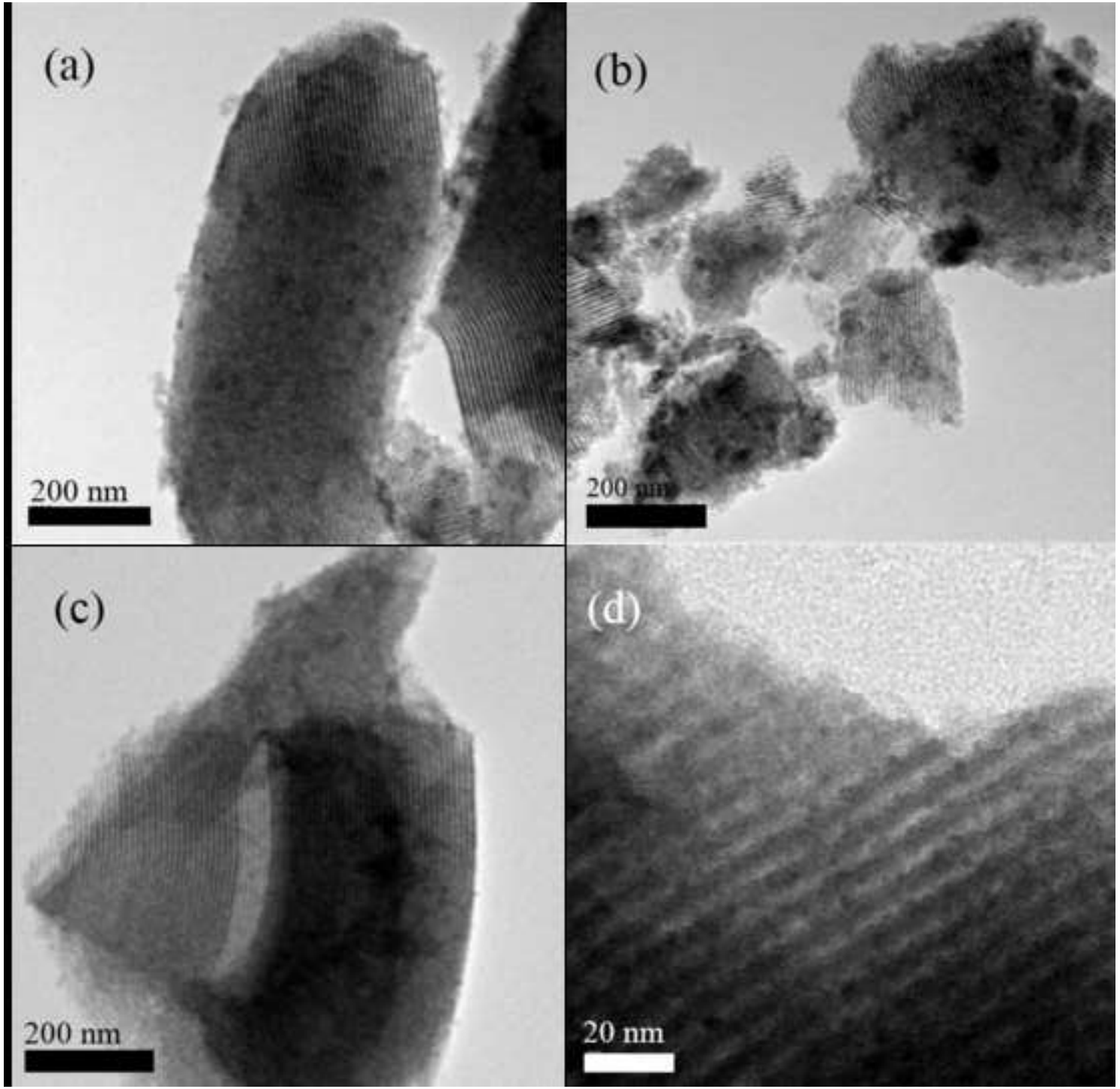

Figure 8

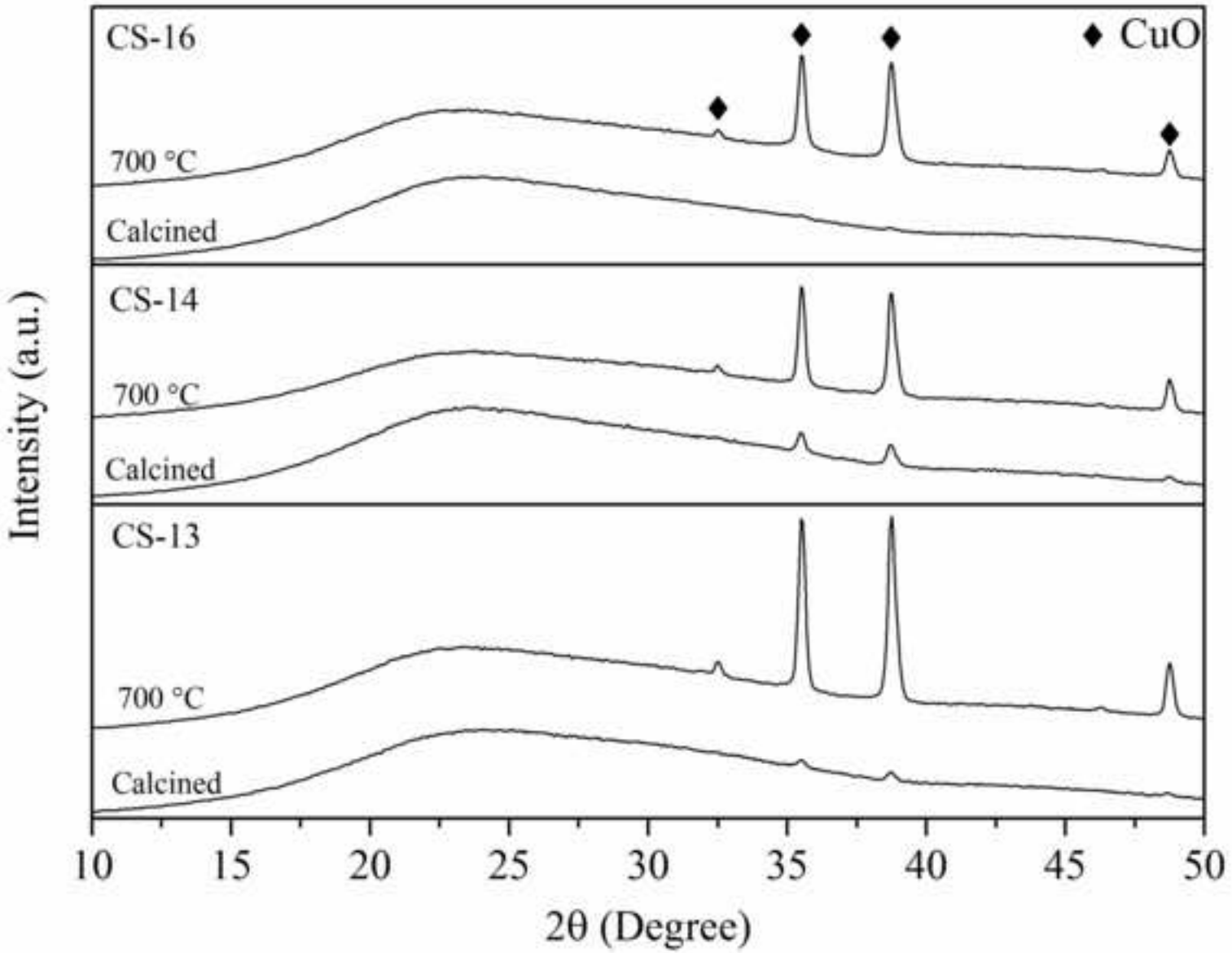
CS-16
CuO
700 °C
Calcined
CS-14
700 °C
Calcined
CS-13
700 °C
Calcined
Intensity (a.u.)
10
15
20
25
30
35
40
45
50
2θ (Degree)

Figure 9

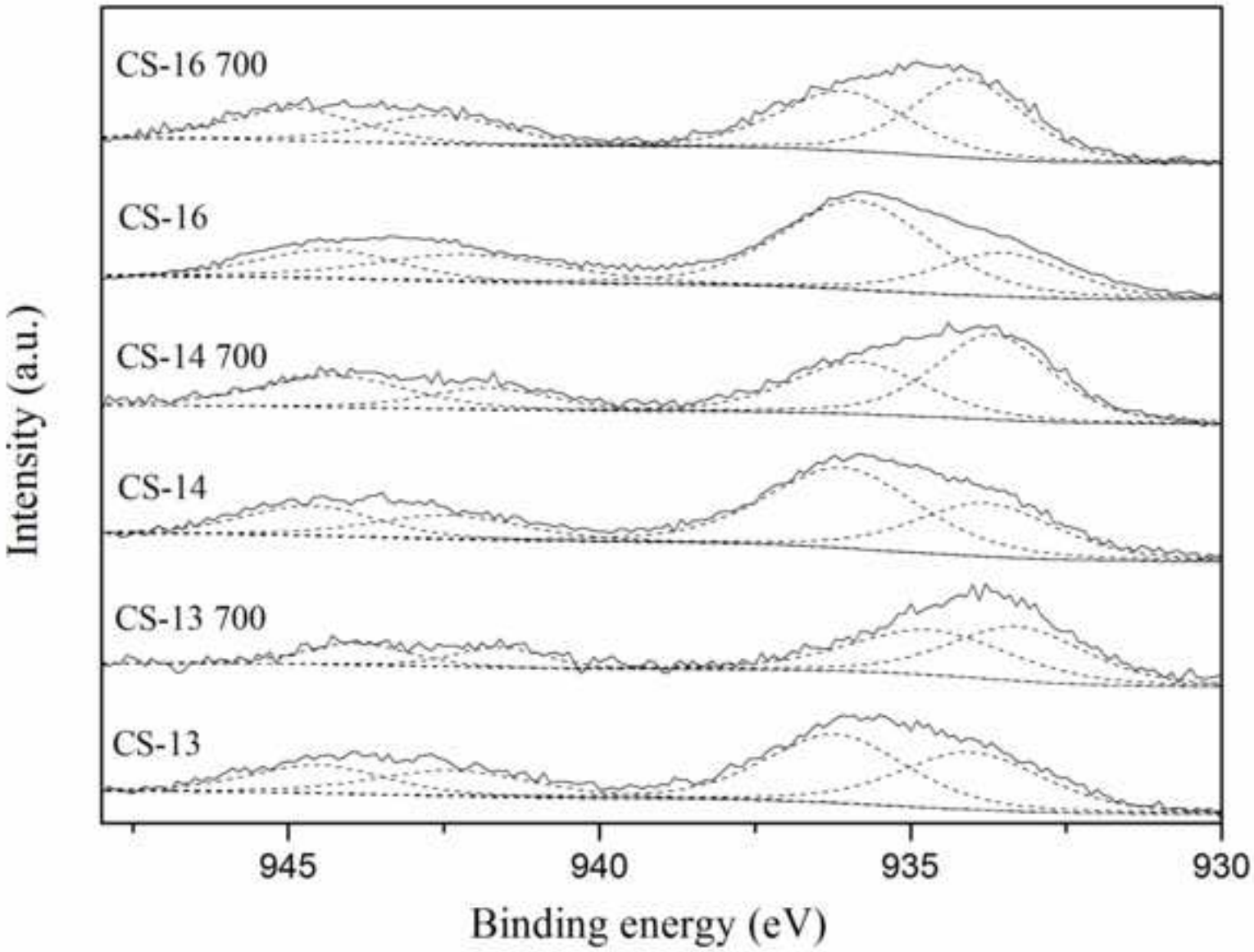
CS-16 700
CS-16
CS-14 700
CS-14
CS-13 700
CS-13
Intensity (a.u.)
945
940
935
930
Binding energy (eV)

Figure 10

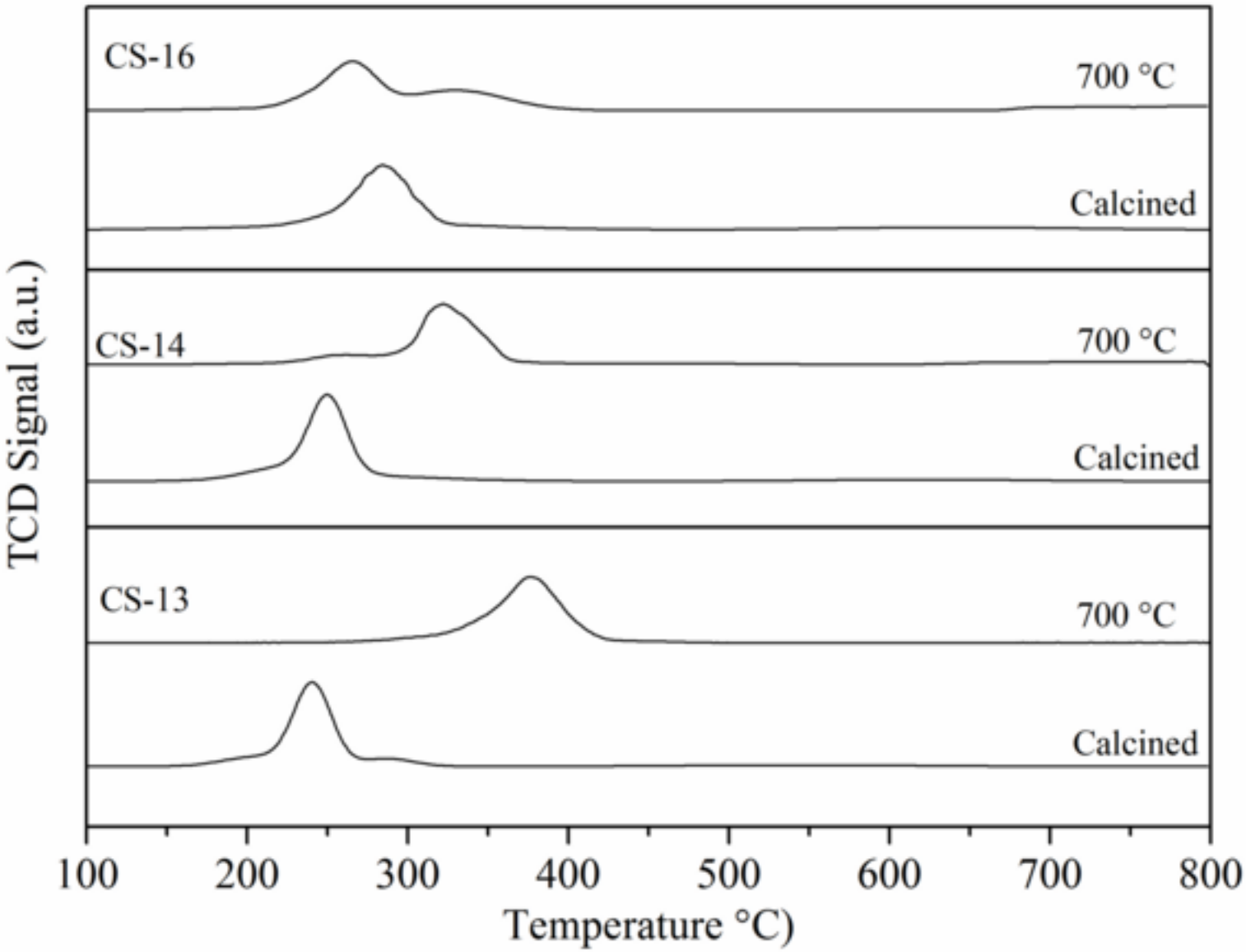
CS-16
700 °C
Calcined
CS-14
700 °C
Calcined
CS-13
700 °C
Calcined
TCD Signal (a.u.)
100
200
300
400
500
600
700
800
Temperature °C)

Figure 11

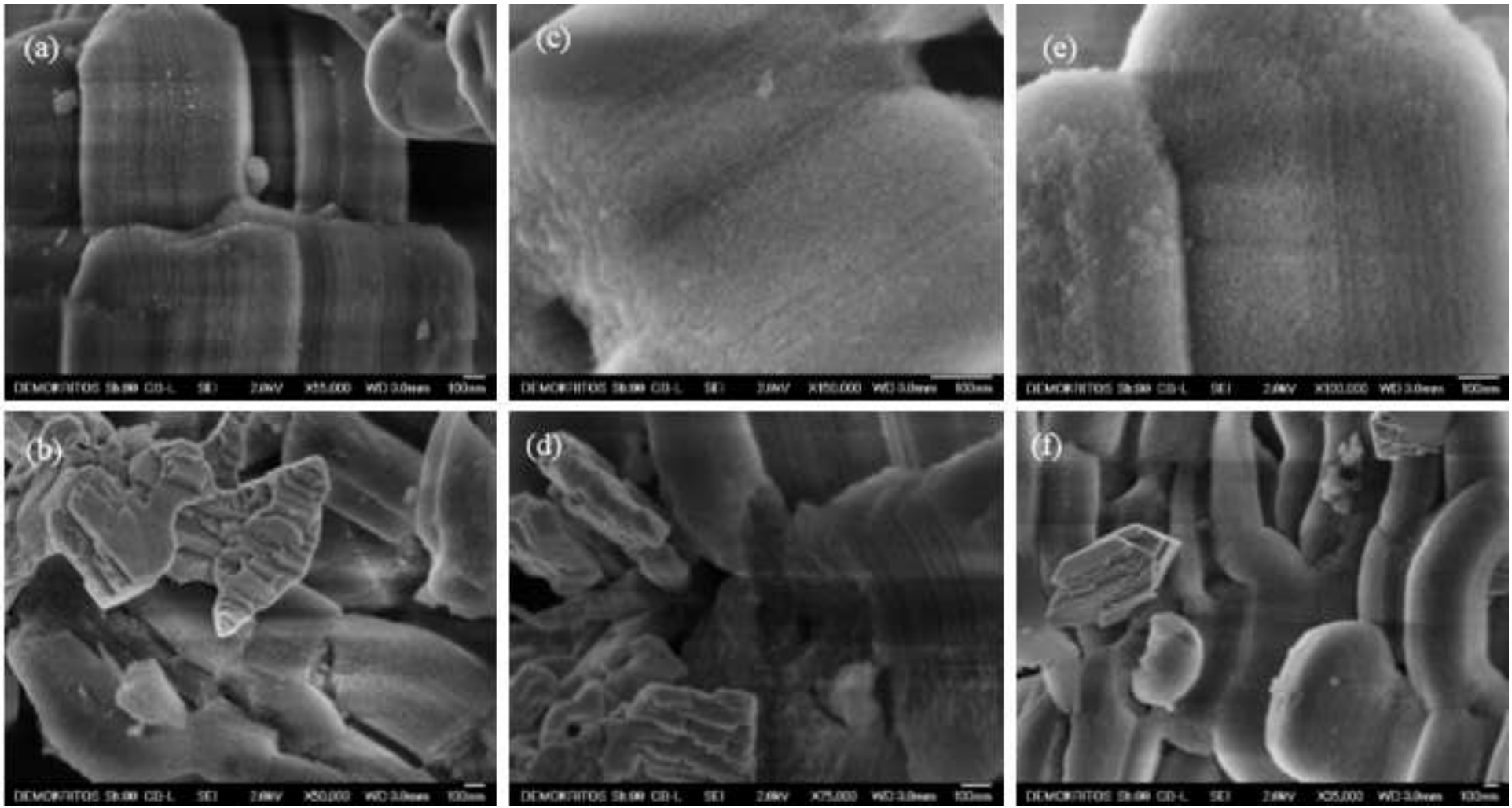

Figure 12a

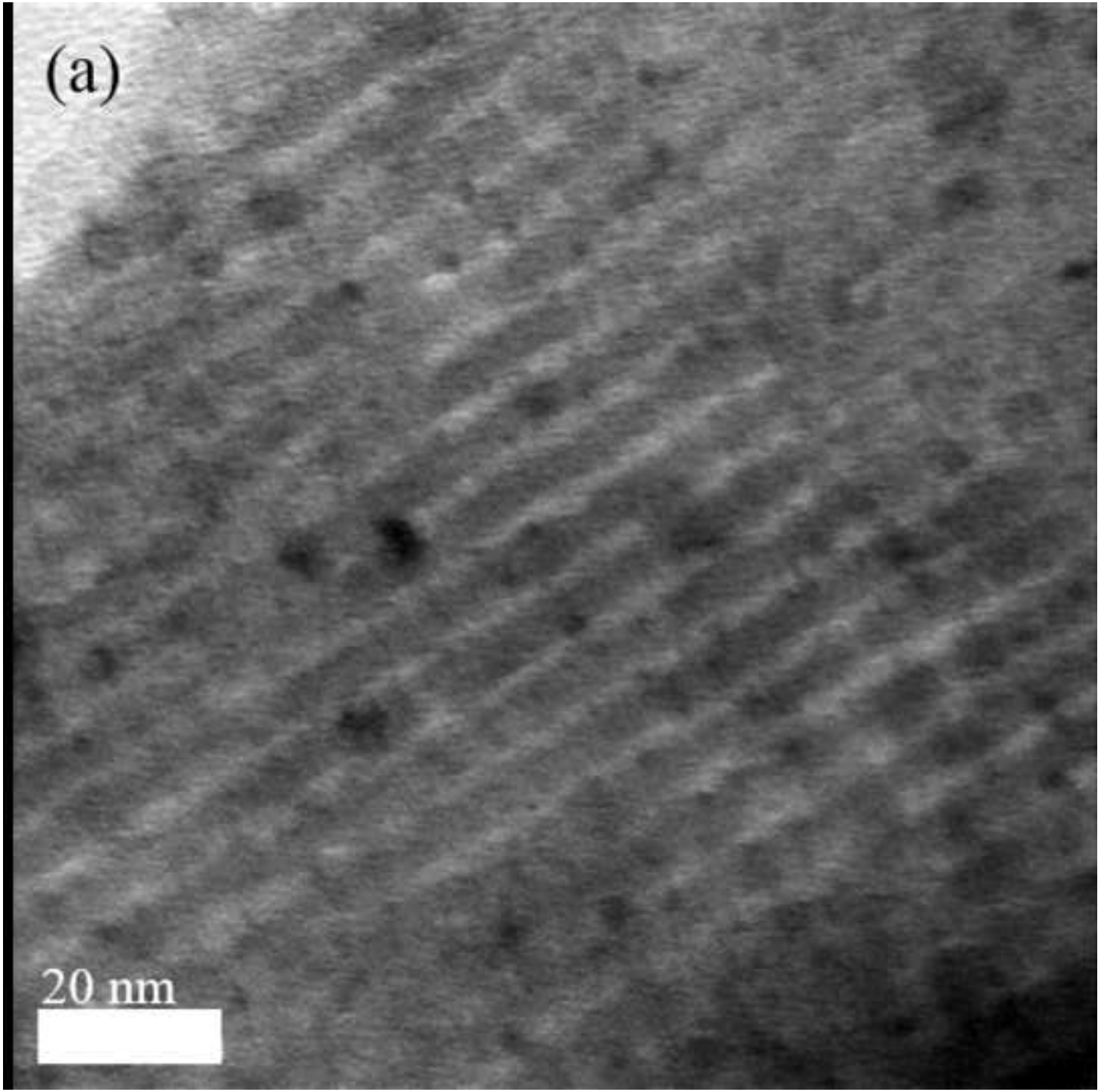

ACCEPTED MANUSCRIPT

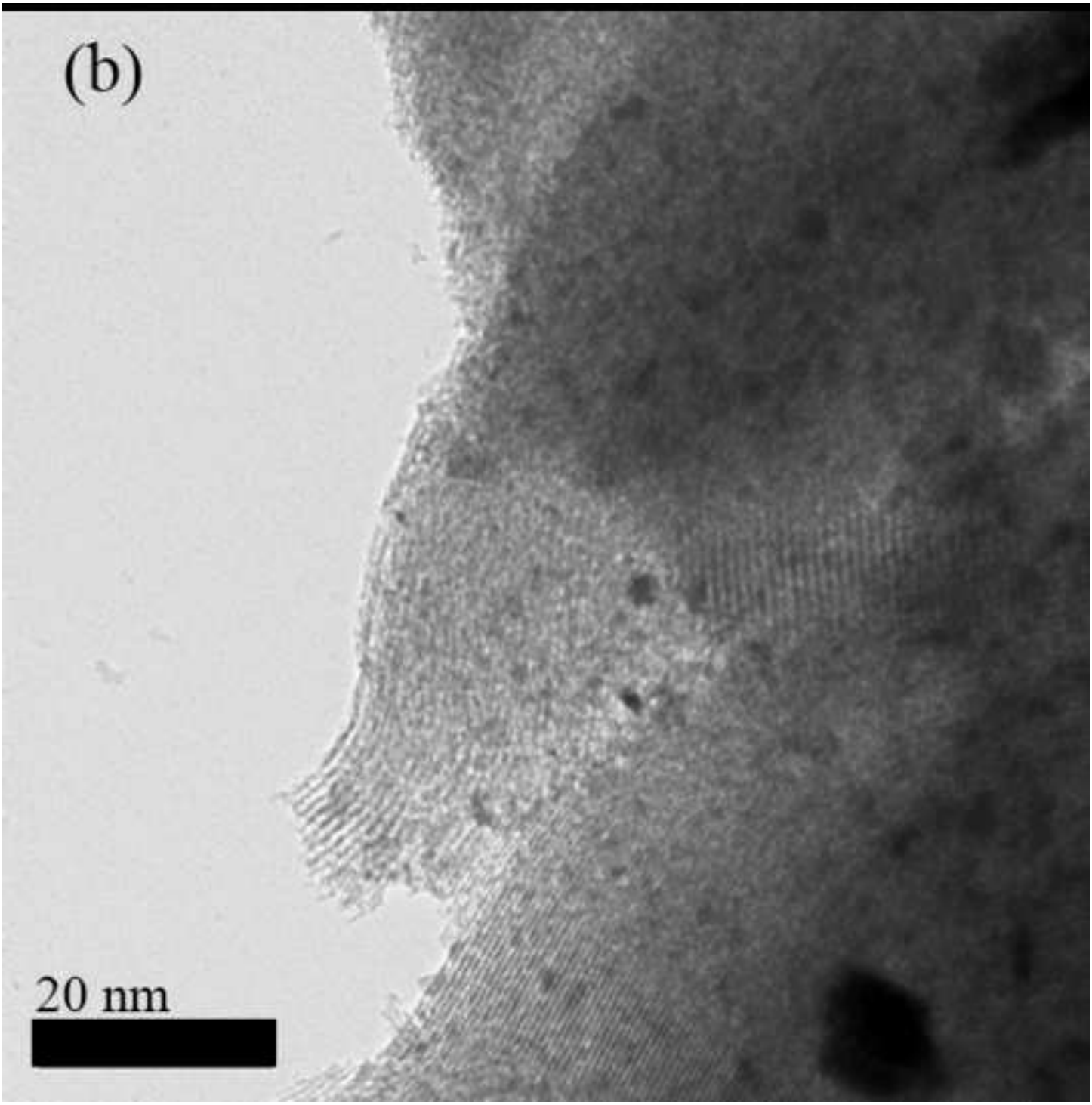

Figure 13a

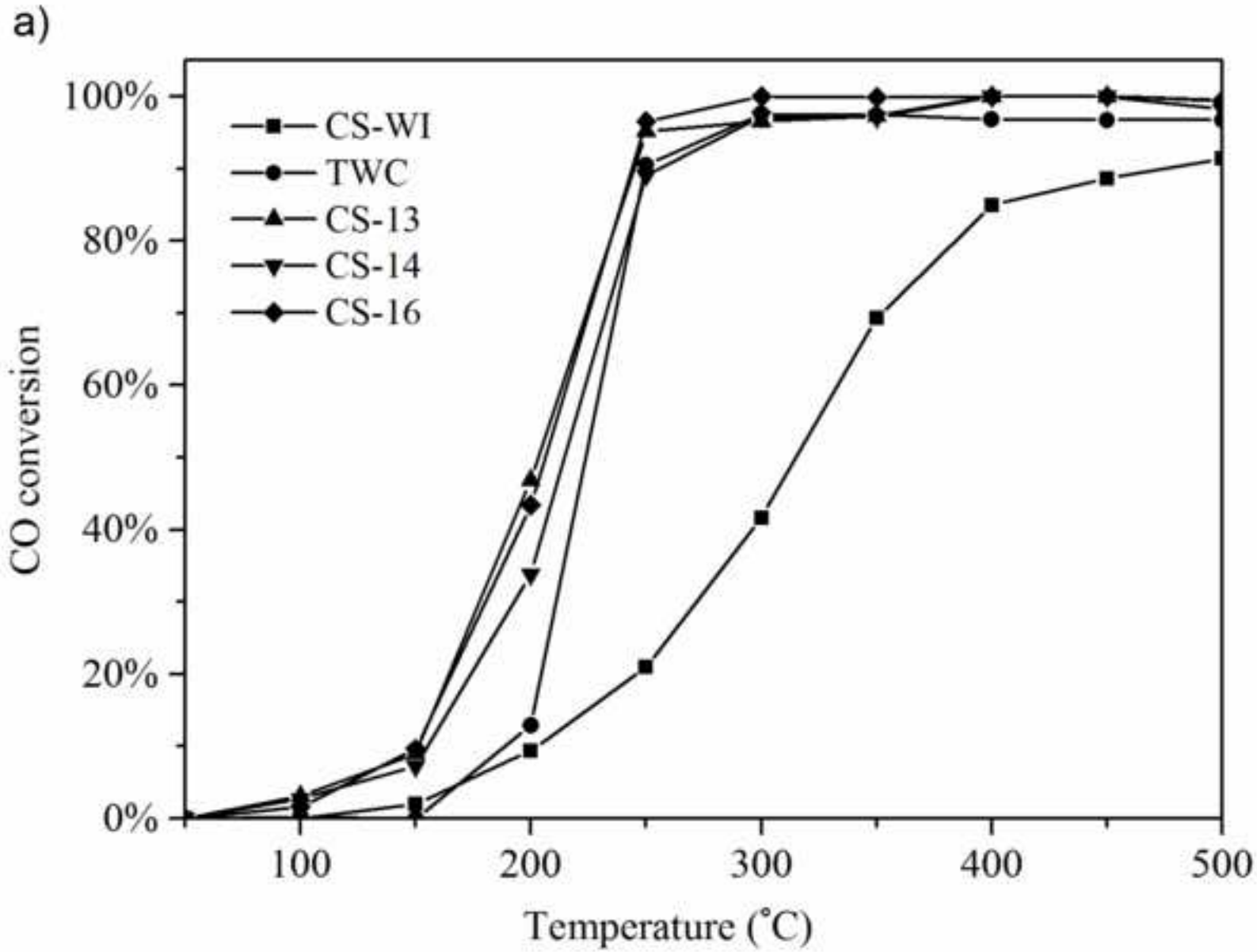
a)
100%
80%
60%
40%
20%
0%
CO conversion
CS-WI
TWC
CS-13
CS-14
CS-16
100
200
300
400
500
Temperature (°C)

Figure 13b

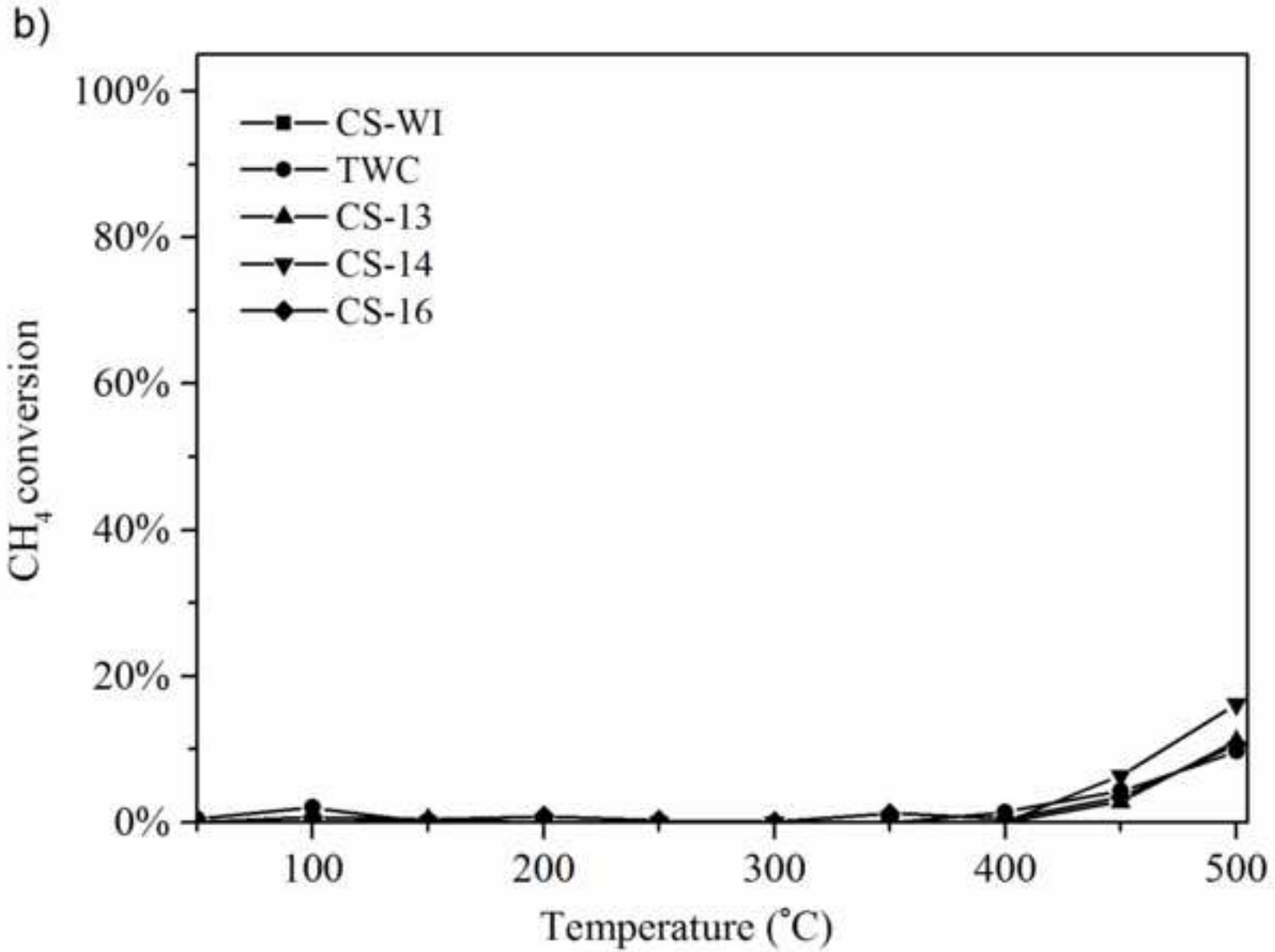
b)
100%
80%
60%
40%
20%
0%
CS-WI
TWC
CS-13
CS-14
CS-16
CH_4 conversion
100
200
300
400
500
Temperature (°C)

Figure 13c

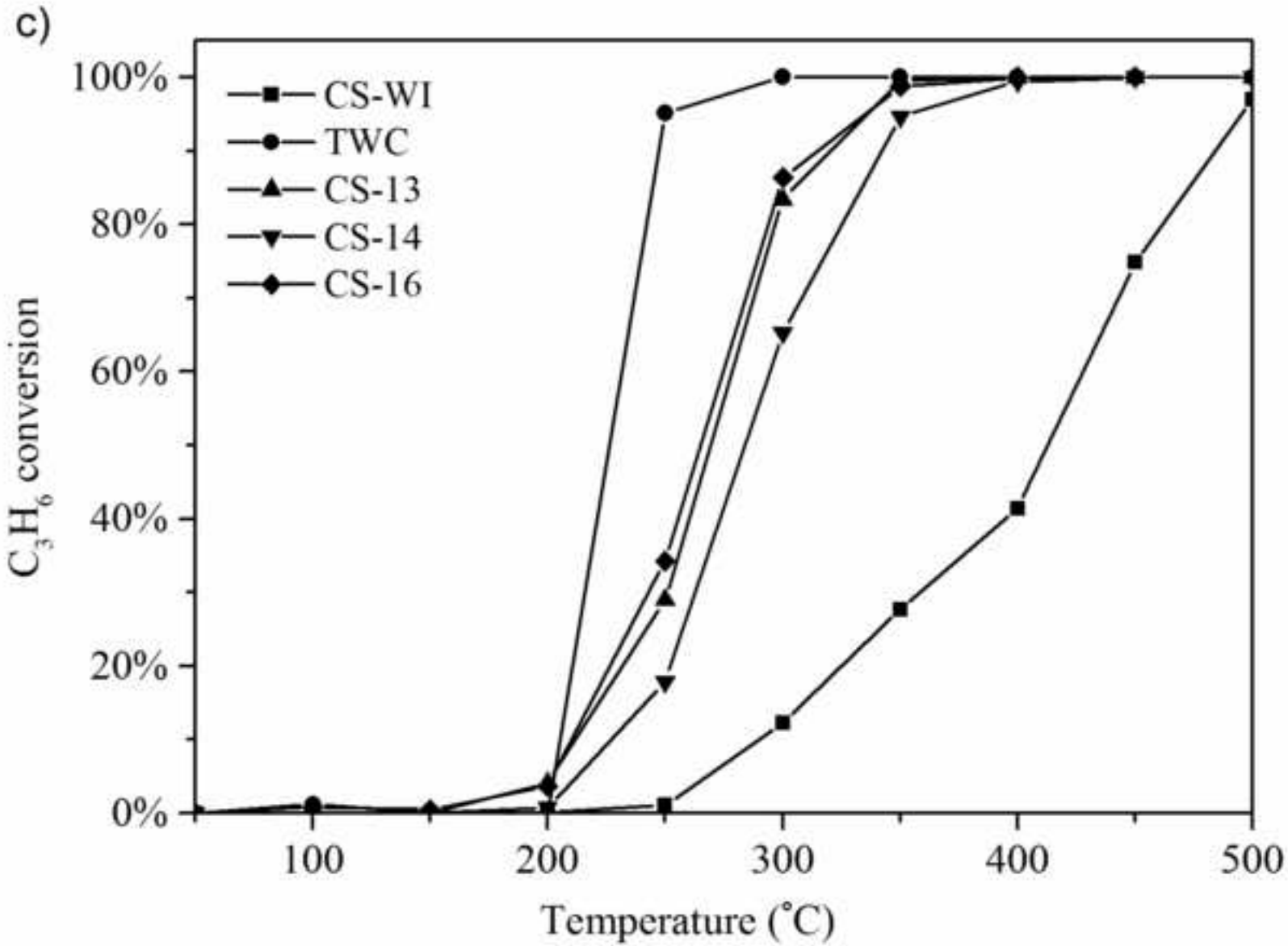
c)
100%
80%
60%
40%
20%
0%
C_3H_6 conversion
CS-WI
TWC
CS-13
CS-14
CS-16
100
200
300
400
500
Temperature (°C)

Figure 13d

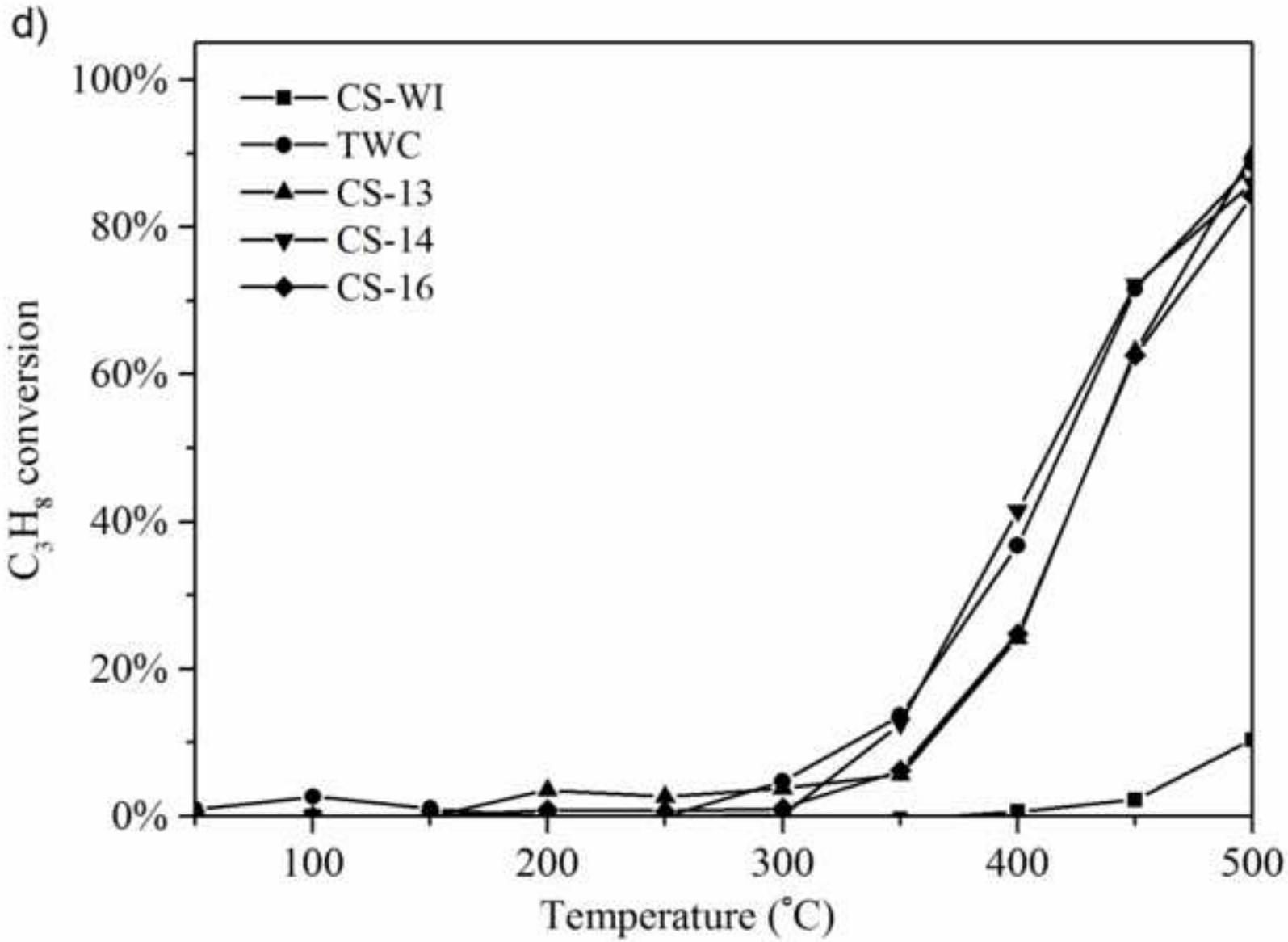
d)
100%
80%
60%
40%
20%
0%
CS-WI
TWC
CS-13
CS-14
CS-16
C_3H_8 conversion
100
200
300
400
500
Temperature (°C)

Figure 13e

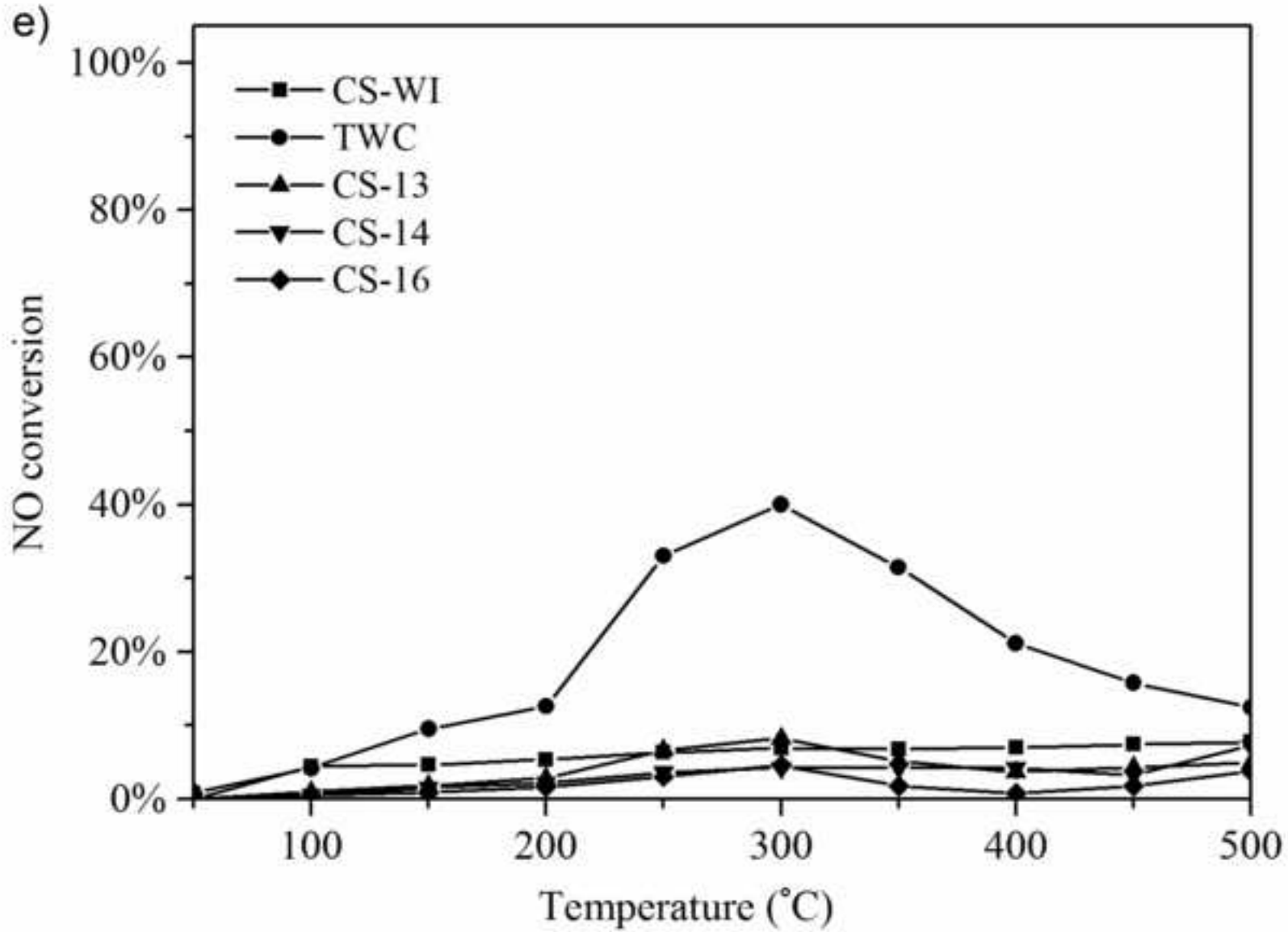
e)
100%
80%
60%
40%
20%
0%
NO conversion
CS-WI
TWC
CS-13
CS-14
CS-16
100
200
300
400
500
Temperature (°C)

Figure 14a

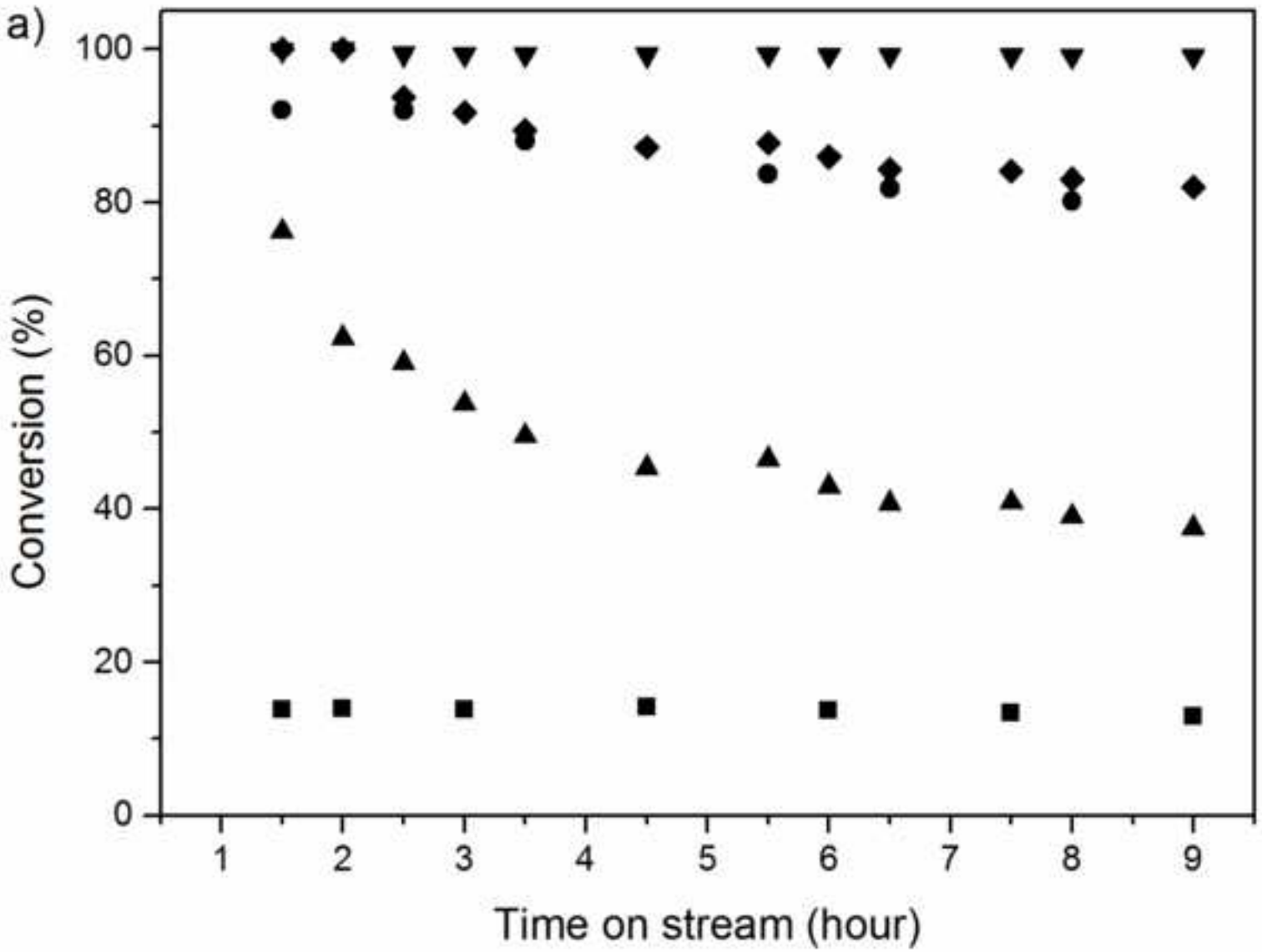

Figure 14b

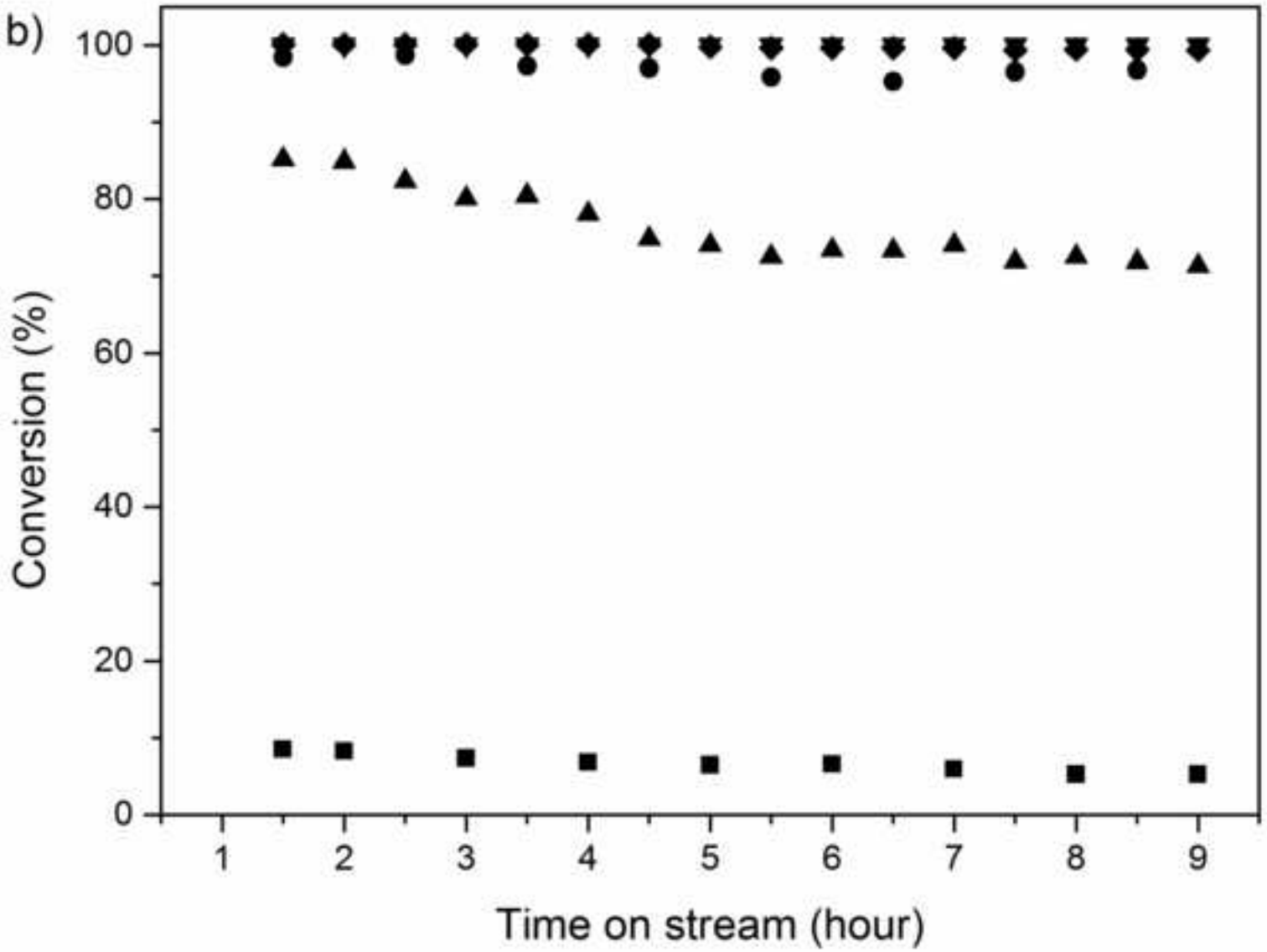

ACCEPTED MANUSCRIPT

Table 1: Composition of the reaction gas mixture in stoichiometric condition, N_2 was used as balance gas.

Gas (vol. %)	CO	CH_4	C_3H_6	C_3H_8	CO_2	H_2O	H_2	O_2	NO
Stoic. condition	0.7	0.0225	0.0450	0.0225	15	10	0.233	0.777	0.1

Table 2: Physicochemical properties of SBA-15 and CuO/SBA-15 prepared with WI method and ADP method with different Cu^{2+}/NH_3 molar ratio after calcination at 550 °C.

Sample	S_{BET}[1] ($m^2\ g^{-1}$)	V_{meso}[2] ($cm^3\ g^{-1}$)	V_{micro}[3] ($cm^3\ g^{-1}$)	d_p[4] (nm)	Cu content[5] (wt. %)	d_{CuO}[6] (nm)	Cu dispersion[7] (%)	d_{Cu}[7] (nm)
SBA-15	910	1.41	0.061	6.2	-	-	-	-
CS-WI	752	1.42	0.011	7.4	9.2	28	0.15	660
CS-13	525	0.94	0.012	7.9	9.1	22	2.5	40.7
CS-14	482	0.88	0.017	8.1	9.4	23	8.4	11.9
CS-16	435	1.18	0.017	9.7	10.1	n.d.	7.7	12.9

[1] B.E.T surface area of the support with non-metal containing support weight. [2] Mesopore volume. [3] Micropore volume via t-plot method. [4] Average pore diameter by applying the Barret-Joyner-Halenda method (BJH) to the adsorption branch of the isotherm. [5] via EPMA. [6] Based on Scherrer equation on CuO (111) diffraction peak. [7] Via N_2O pulse titration.

Table 3: XPS analysis of CuO/SBA-15 catalyst prepared with different Cu^{2+}/NH_3 molar ratio after calcination at 550 °C and after thermal treatment of 700 °C.

	$Cu2p_{3/2}$ peak 1		$Cu2p_{3/2}$ peak 2		Cu/Si atomic ratio
	Position (eV)	Relative intensity (%)	Position (eV)	Relative intensity (%)	
CS-13	934.0	47	936.2	53	0.090
CS-13 700	933.3	51	934.7	49	0.032
CS-14	933.8	38	936.1	62	0.088
CS-14 700	933.7	56	935.9	44	0.050
CS-16	933.5	31	935.9	69	0.092
CS-16 700	934.1	54	936.1	46	0.061

ACCEPTED MANUSCRIPT

Table 4: Relative TPR peak area of the prepared catalyst with different Cu^{2+}/NH_3 molar ratio after calcination at 550 °C and after thermal treatment of 700 °C.

Catalyst	d_{CuO}[1] (nm)	Relative peak area from TPR (%)			
		α_1	α_2	β	γ
CS-13	22	5	80	8	7
CS-13 700	25	n.d.	4	94	n.d.
CS-14	23	7	81	5	7
CS-14 700	25	n.d.	14	76	10
CS-16	n.d.	6	82	5	7
CS-16 700	24	n.d.	56	33	1

[1] Based on Scherrer equation on CuO (111) diffraction peak.

Table 5: Activity test: catalysts' light-off temperature (T_{50}) and maximum conversion of each component.

Component	TWC		CS-WI		CS-13		CS-14		CS-16	
	T_{50} (°C)	C_{max} (%)	T_{50} (°C)	C_{max} (%)	T_{50} (°C)	C_{max} (%)	T_{50} (°C)	C_{max} (%)	T_{50} (°C)	C_{max} (%)
CO	222	97	312	91	204	100	215	100	207	100
CH_4	-	10	-	0	-	11	-	16	-	11
C_3H_6	225	100	430	97	269	100	284	100	265	100
C_3H_8	370	89	-	10	433	90	420	86	433	84
NO	-	40	-	7	-	8	-	4	-	6